UNIVERSITÉ DE GENÈVE
INSTITUT DES SCIENCES DE L'ENVIRONNEMENT

International Energy Agency

Five satellite products deriving beam and global irradiance validation on data from 23 ground stations

Pierre Ineichen
University of Geneva

February 2011

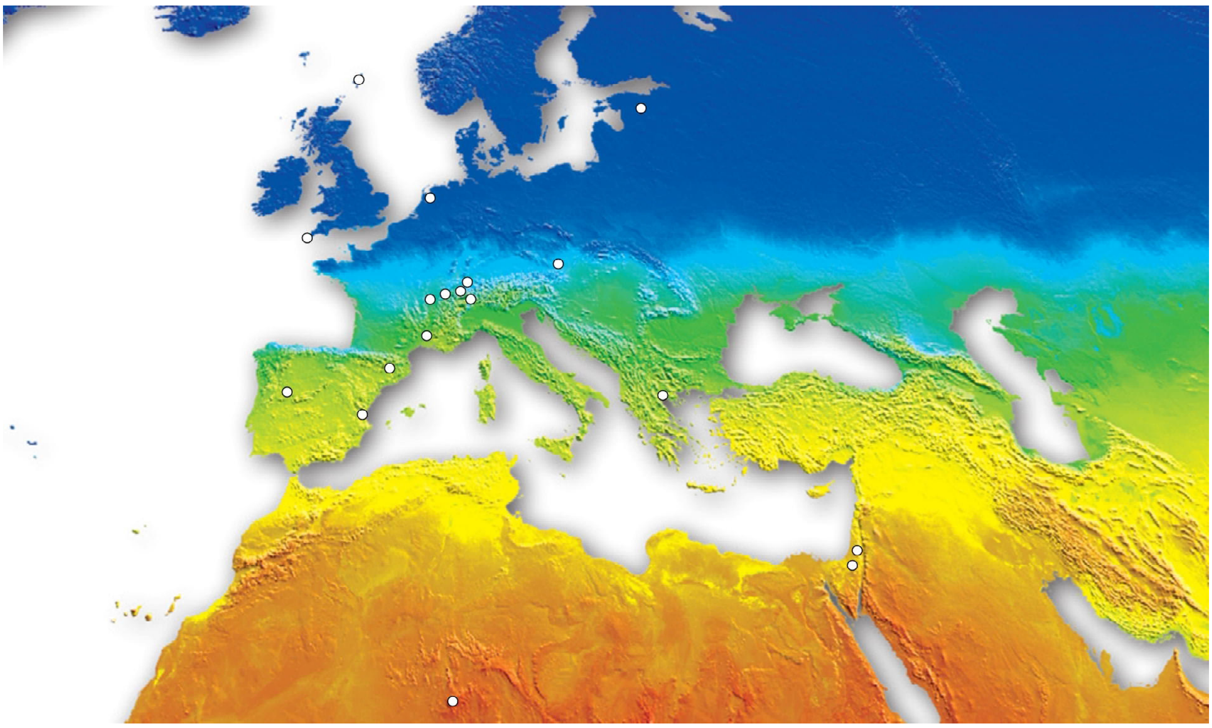

Irradiance map produced by 3Tier

Five satellite products deriving beam and global irradiance validation on data from 23 ground stations

Pierre Ineichen
University of Geneva
February 2011

Abstract

Models converting satellite images into the different radiation components become increasingly performing and give often better estimation of the solar irradiance availability than ground measurements if the station is not situated in the near vicinity of the application.

Five different satellite products deriving both global and beam irradiance are validated against data from 23 ground sites. The main conclusions are:

- the global irradiance is retrieved with a negligible bias and an average standard deviation around 16% for the best algorithm. For the beam irradiance, the bias is around several percents, and the standard deviation around 35%,
- the main deviation comes from the knowledge of the aerosol optical depth,
- the high latitude sites give not poorer results than the other sites,

The interannual variability of the irradiance conditions, the lack of independent ground measurements such as aerosol data, the difficulty to assess the exact calibration of the ground data, and the choice of a specific year to carry out the validation, conduct to results that give good indications, but from which it is difficult to draw general conclusions.

1. Introduction

Models converting satellite images into the different radiation components become increasingly performing and give often better estimation of the solar irradiance availability than ground measurements if the station is not situated in the near vicinity of the application (Zelenka, 1999). If the global irradiance can be derived with a good accuracy, it is more difficult for the beam component and the dispersion of the models is higher.

The aim of the present study is to validate and compare five different products deriving the global and beam irradiance components from meteorological satellite images. It is a complement to a previous study conducted by the author (Ineichen 2009) on products from Eumetsat Satellite Application Facilities (SAF). These algorithmes are derived by GeoModel in Bratislava (SolarGis), Helioclim Soda (heliosat 3v3), 3Tier company in the United States, University of Oldenburg (EnMetSol-Solis and EnMetSol-Dumortier) and the IrSolAv company in Spain.

2. Ground data

The ground data used in the study are acquired at stations part of networks such as Baseline Solar Radiation Network (BSRN), Commission International de l'Eclairage (CIE), FluxNet network, Swiss Institute of Meteorology (ISM-Anetz) and World Radiation Data Center (WRDC). Data from 23 ground sites situated mainly on the European continent are used. The work is done on data covering the year 2006.

Beside the global horizontal irradiance G_h, half of the sites acquire the normal beam irradiance B_n. High precision instruments (WMO 2008) such as Kipp and Zonen CM10

Station	Country	Climate	D_h	B_n	latitude °	longitude °	altitude m	operated by
Cabauw	The Netehrlands	temperate maritime		x	51.970	4.930	2	BSRN - KNMI
Camborne	United Kingdom	temperate maritime		x	50.220	-5.310	88	BSRN - Met Office
Carpentras	France	mediterranean		x	44.080	5.060	100	BSRN - Météo France
Davos Dorf	Switzerland	semi-continental alpin		x	46.810	9.840	1610	WRDC - Met Office
El Saler	Spain	semi arid, warm summer			39.346	-0.319	10	FluxNet
Geneva	Switzerland	semi-continental		x	46.199	6.131	420	CIE - UNIGE
Jungfraujoch	Switzerland	high alpine		x	46.550	7.980	3571	CLIMAP - Météo Suisse
Las Majadas	Spain	semi arid, warm summer			39.942	-5.773	260	FluxNet
Lerwick	United Kingdom	cold oceanic		x	60.130	-1.180	82	BSRN - Met Office
Locarno	Switzerland	warm temperate, humid			46.170	8.780	367	ANETZ - Météo Suisse
Nantes	France	oceanic	x		47.150	-1.330	30	CIE - CSTB
Payerne	Switzerland	moderate maritime/continental		x	46.820	6.950	490	BSRN - Météo Suisse
Sede Boqer	Israel	dry steppe			30.867	34.767	457	BSRN - Met Office
Sion	Switzerland	dry alpine			46.220	7.330	489	ANETZ - Météo Suisse
Sonnblick	Austria	temperate alpine	x		47.050	12.950	3105	WRDC - ZAMG
Tamanrasset	Algeria	hot, dry desert			22.780	5.520	1400	BSRN - Met Office
Thessaloniki	Greece	mediterranean temperate		x	40.630	22.970	60	WRDC - Met Office
Toravere	Estonia	cold humid		x	58.270	26.470	70	BSRN - EMHI
Val Alinya	Spain	warm temperate, humid			42.152	1.449	1770	FluxNet
Vaulx-en-Velin	France	semi-continental	x		45.780	4.930	170	CIE - ENTPE
Wien / Hohe Warte	Austria	continental	x		48.250	16.350	203	WRDC - ZAMG
Yatir Forest	Israel	hot arid			31.347	35.052	650	FluxNet
Zürich	Switzerland	temperate atlantic			47.475	8.530	558	ANETZ - Météo Suisse

ANETZ	MeteoSwiss network	CUEPE	Energy Group, UniGe
BSRN	Baseline Surface Radiation Network	EHMI	The Estonian Meteorological and Hydrological Institute
CIE	Commission Internationale pour l'Eclairage	ENTPE	Ecole Nationale des Mines de Paris
CLIMAP	MeteoSwiss Climate Maping application	KNMI	The Netherlands Institute of Meteorology
CSTB	Centre Scientifique et Technique du Bâtiment	UNIGE	University of Geneva
		ZAMG	Zentralanstalt für Meteorologie und Geophysik/Geodynamik

Table I List of the stations, data and parameters availability.

and Eppley PSP pyranometers, and Eppley NIP pyrheliometers, are used to acquire the data. A stringent calibration, characterization and quality control was applied on all the data by the person in charge of the measurements, the coherence of the data for all the stations was verified by the author and is described in the following section. For two sites, the aerosol optical depth *aod* and the water vapor column *w* is independently acquired and is used as input to clear sky models in order to assess the instruments calibration factors.

The climate, latitude, longitude and altitude of the stations are given in Table I.

3. Data quality control

For all the stations, the first quality control consist of an assessment of the acquisition time stamp. To point out a possible time shift in the data, the symmetry in solar time of the irradiance for very clear days is visually checked. The horizontal global and if available, the normal beam irradiances are plotted versus the sinus of the solar elevation angle for specific clear days. If the time stamp is correct, the afternoon curve should lay over the morning curve as visualized on Figure 1a.

If this test is positive, a verification can be done with the help of the global clearness index K_t defined as:

$$K_t = \frac{G_h}{I_o \cdot \sin(h)}$$

where G_h is the horizontal global irradiance, I_o is the solar constant, and h the solar elevation angle. The clearness index is plotted for the morning and the afternoon data in a separate color. The upper limit, representative of clear sky conditions, should lay

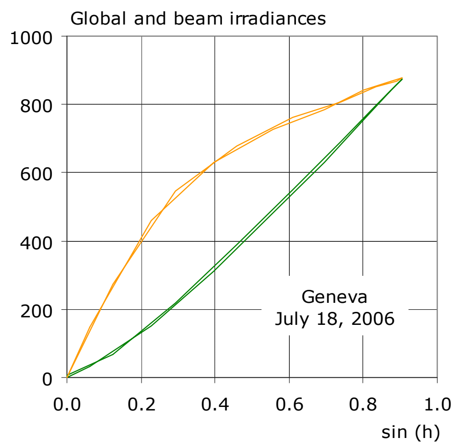

Figure 1a The global horizontal and normal beam irradiances are represented versus the sinus of the solar elevation angle for a clear day.

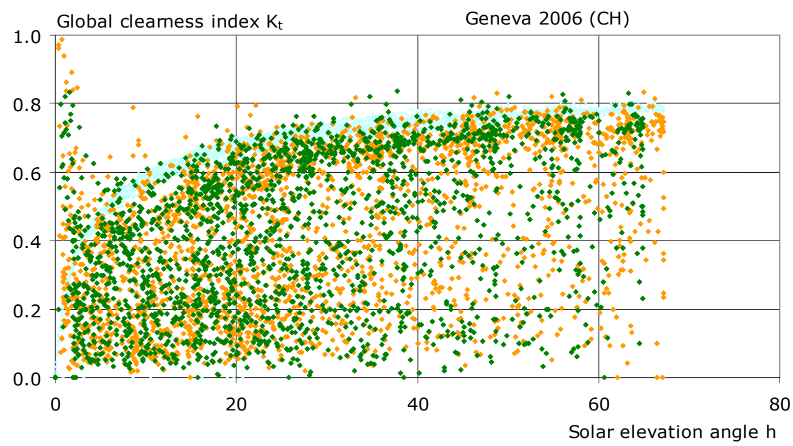

Figure 1b The global clearness index K_t is represented separately for the morning (green) and the afternoon (yellow) data, versus the solar elevation angle for one year in hourly values.
Clear sky model data are represented in blue.

over for the morning and the afternoon data as represented on Figure 1b for one year of data acquired at the site of Geneva for the year 2006. Hourly clear sky condition values are plotted in light blue on the same graph. When these two conditions are fulfilled, the time stamp of the data bank is correct, and the solar geometry can be precisely calculated. This test is very sensitive and a time shift of only a few minutes will conduct to an visible assymetry. A similar test can be done with the beam clearness index K_b defined as:

$$K_b = \frac{B_n}{I_o}$$

but this parameter is less sensitive to a possible time shift.

The coherence test between the two components can be verified with the help of the global and beam clearness indices (Ineichen 2010). The hourly beam clearness index is plotted versus the corresponding global index as illustrated on Figure 2 for the site of Carpentras. On the same graph, the clear sky data evaluated with the Solis clear sky model (Müller 2004, Ineichen 2008a) are represented for four different values of aerosol optical depth (*aod*). The more usual corresponding Linke turbidity coefficient T_{Lam2} retrieved from the beam irradiance:

$$B_n = I_o \ e^{(-\delta_{cda} \cdot T_{Lam2} \cdot MA)}$$

and evaluated at air mass AM = 2 is also given on the graph (Linke 1922, Ineichen 2008b). δ_{cda} is the optical depth of a clean and dry atmosphere. An important deviation from the clear sky lines can indicate calibration uncertainties, beam irradiance missalignement or soiled sensors.

The absolute sensor calibration can be assessed with the help of a clear sky model when the atmospheric aerosol optical depth and the water vapor column are known. These two parameters are normally retrieved from spectral measurements. When the

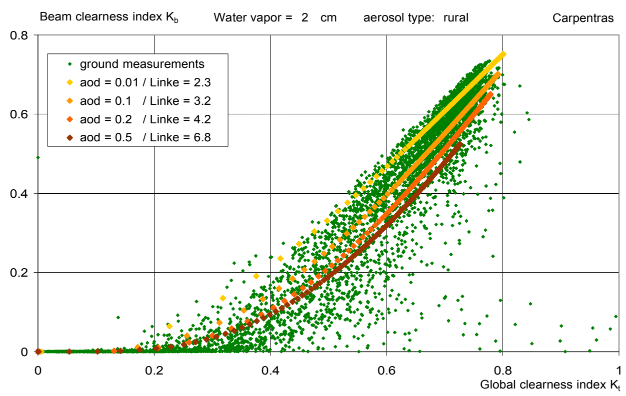

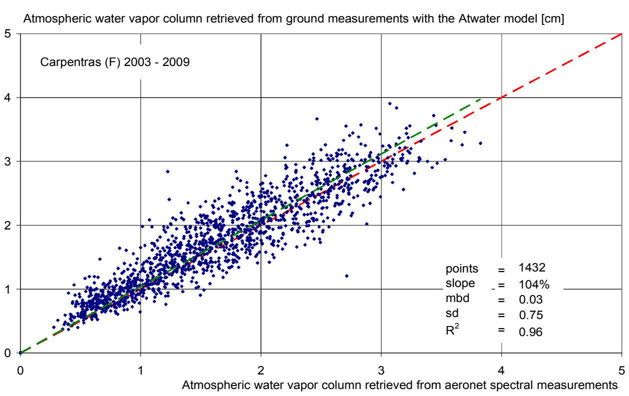

Figure 2 The beam clearness index is plotted against the global clearness index. On the same graph, clear sky modelled values are represented for 4 different aerosol loads

Figure 3 Atmospheric water vapor column evaluated from the ambiant temperature and relative humidity against the watre vapor retrieved from spectral measurements.

water vapor *w* is missing, it can be evaluated from the ground ambiant temperature (T_a) and relative humidity (*HR*) by the use of Atwater model (Atwater 1976) with a good precision as illustrated on Figure 3 for the site of Carpentras and data acquired from 2003 to 2009.

For some sites, the *aod* measurements retrieved from independent networks such as aeronet are acquired as soon as direct sun is available; these values are then averaged to give a daily value and used with the Solis clear sky model to evaluate hourly clear sky G_h and B_n values.

Day by day, the highest hourly value is then selected from the measurements and plotted against the day of the year on Figure 4. These points are representative of the clearest daily sky conditions. Based on the *aod* and water vapor content *w* of the atmopshere, the corresponding clear sky values are evaluated with the model. As the highest values for each day is selected, the upper limit for these two series shoud lay together if the two sets of measurements (irradiance and *aod*) are coherent. On the same graph are also represented the daily clear sky indices defined as:

$$K_h = \frac{\sum_{day} G_h}{\sum_{day} G_{hc}} \quad \text{and} \quad K_{hb} = \frac{\sum_{day} B_n}{\sum_{day} B_{nc}}$$

These values, if the data are coherent, should have an upper limit near of the unity.

4. The clearness index K_t and sky type classification

As it is the case for the majority of the national networks, the global irradiance is the only available measured parameter concerning the solar radiation. Even if for half of the stations the beam component is available, the global irradiance and the corresponding

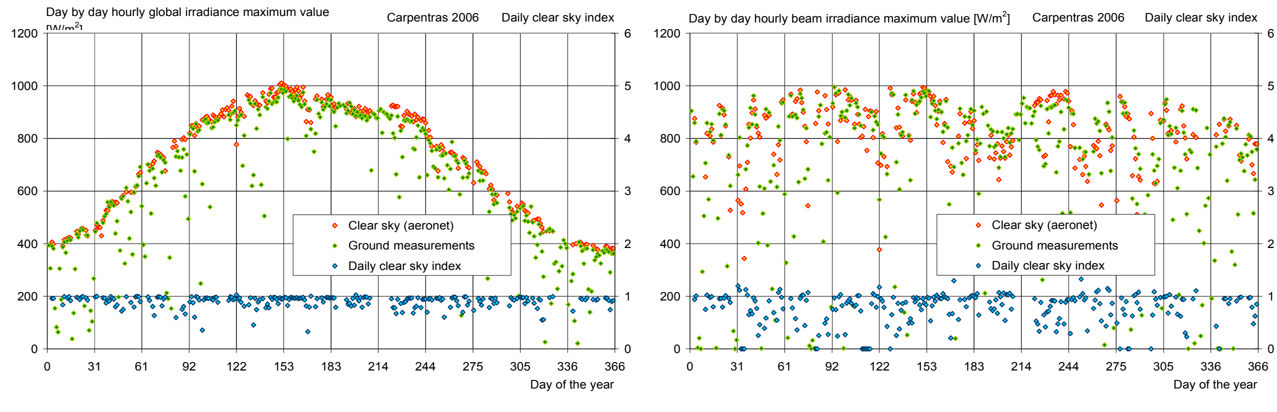

Figure 4 Daily highest value of the global irradiance reported versus the day of the year for the station of Carpentras, for the measurements and the corresponding clear sky evaluated from the aod and the Solis model. The daily clear sky index is also represented.

clearness index K_t are key parameters in the field of irradiance modelization. The clearness index K_t was introduced as a norm (Black 1954) to characterize the insulation conditions at a given point in time when only the global component is known. Unfortunately, this parameter is not independent of the solar elevation angle as it is shown on the left graphe of Figure 5 where the clearness index K_t is plotted versus the solar elevation angle for the site of Carpentras. It can be seen on this Figure that clear sky conditions, determined by the upper limit of the clearness index values, are not equally represented by K_t for the different solar elevation angles.

In order to use the clearness index as a reliable sky condition descriptor, Perez et al. (1990) modified this parameter to make it independent of the solar elevation angle. The formulation is the following:

$$K_t' = \frac{K_t}{(1.031 \cdot \exp(-1.4 / (0.9 + 9.4 / AM)) + 0.1)}$$

where *AM* is the optical air mass as defined by Kasten (1980). This modified clearness index is represented on Figure 5 (right graph) for the same points than above. It can clearly be seen on this Figure that even if some patterns are still present, the modified clearness index is relatively independent from the solar elevation angle. Therefore, it is now possible to define three zones to characterize three sky types:

clear sky conditions	$0.65 < K'_t \leq 1.00$
intermediate sky conditions	$0.30 < K'_t \leq 0.65$
cloudy sky conditions	$0.00 < K'_t \leq 0.30$

These limits are arbitrary, but are coherent with other classifications, like for example the Cloud Free Index saturation (CFIsat) as defined by Dürr (2006):

$$CFIsat = 100\ (CFI - 1)\ /\ z$$

where z and *CFI* are defined in Dürr (2004). CFIsat is independent from the irradiance measurements; it is a function of the downward surface longwave irradiance and the dry bulb temperature. The comparison between the *CFIsat* and K'_t is illustrated on Figure 6 (right graph). The red dashed lines represent the limits used in the present study and applied on the modified clearness index. In the *CFIsat* classification, clear sky conditions are defined by a *CFIsat* below 0%, and cloudy conditions above 50%. The corresponding limits are represented in blue dashed lines. It can be seen on Figure 6 that the majority of the points are situated in the intersections of the corresponding three zones.

Another assessement can be done with the cloud cover as illustrated on Figure 6 (left graph). Here also, the limits used in the present study are well correlated with the cloud

Figure 5 Global and modified clearness index versus the solar elevation angle.

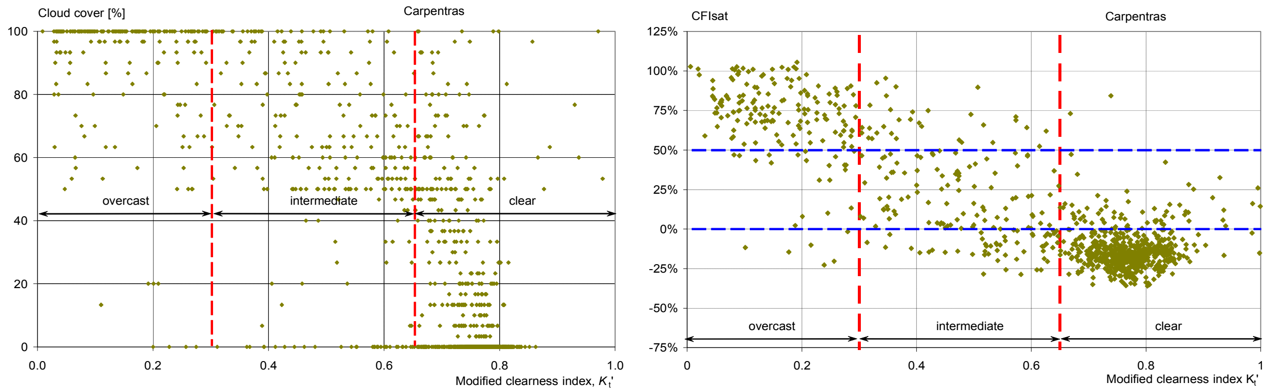

Figure 6 Cloud cover and *CFIsat* coefficient versus the modified clearness index. The sky condition selection limits are represented in dashed red lines.

cover (0% cloud cover for the clear sky conditions and 100% cloud cover for the overcast sky conditions).

5. Satellite derived data

Five different products are validated in the present study. The methodology and the input parameters are described in the following section. The product from University of Oldenburg (EnMetSol) is evaluated for two different aerosol climatologies.

5.1 SolarGis

The irradiance components are the results of a five steps process: a multi-spectral analysis classifies the pixels, the lower boundary (LB) evaluation is done for each time slot, a spatial variability is introduced for the upper boundary (UP) and the cloud index definition, the Solis clears sky model is used as normalization, and a terrain disaggregation is finally applied.

Four MSG spectral channels are used in a classification scheme to distinguish clouds from snow and no-snow cloud-free situations. Prior to the classification, calibrated pixel values were transformed to three indices: normalized difference snow index (Ruyter 2007), cloud index (Derrien 2005), and temporal variability index. Exploiting the potential of MSG spectral data for snow classification removed the need of additional ancillary snow data and allowed using spectral cloud index information in cases of complex conditions such as clouds over high albedo snow areas.

In the original approach by Perez (2002), the identification of surface pseudo-albedo is based on the use of a lower bound (LB), representing cloudless situations. This approach neglects diurnal variability of LB that is later corrected by statistical approach. Instead of identifying one value per day, LB is represented by smooth 2- dimensional surface (in day and time slot dimensions) that reflects diurnal and seasonal changes in LB and reduces probability of no cloudless situation.

Overcast conditions represented in the original Perez model by a fixed Upper Bound (UB) value were updated to account for spatial variability which is important especially in the higher latitudes. Calculation of cloud index was extended by incorporation of snow classification results.

The broadband simplified version of Solis model (Ineichen 2008a) was implemented. As input of this model, the climatology values from the NVAP water vapor database (Randl 1996) and Atmospheric Optical Depth data by (Remund 2008) assimilated with Aeronet and Aerocom datasets are used.

Simplified Solis model was also implemented into the global to beam Dirindex algorithms to calculate Direct Normal Irradiance component (Perez 1992, Ineichen 2008c). Diffuse irradiance for inclined surfaces is calculated by updated Perez model (1987).

Processing chain of the model includes post-processing terrain disaggregation algorithm based on the approach by Ruiz-Arias (2010). The disaggregation is limited to shadowing effect only, as it represents most significant local effect of terrain. The algorithm uses local terrain horizon information with spatial resolution of 100 m. Direct and circumsolar diffuse components of global irradiance were corrected for terrain shadowing.

5.2 Heliosat-2 algorithm

The Helioclim 3 data bank is produced with the Heliosat-2 method that converts observations made by geostationary meteorological satellites into estimates of the global irradiation at ground level. This version integrates the knowledge gained by various exploitations of the original Heliosat method and its varieties in a coherent and thorough way.

It is based upon the same physical principles but the inputs to the method are calibrated radiances, instead of the digital counts output from the sensor. This change opens the possibilities of using known models of the physical processes in atmospheric optics, thus removing the need for empirically defined parameters and of pyranometric measurements to tune them. The ESRA models (ESRA 2000, Rigollier 2000 and 2004) are used for modeling the clear-sky irradiation. The assessment of the ground albedo and the cloud albedo is based upon explicit formulations of the path radiance and the transmittance of the atmosphere. The turbidity is based on climatic monthly Linke Turbidity coefficients data banks.

The Liu and Jordan (1960) model is used to split the global irradiance into the diffuse and beam components.

5.3 3Tier algorithm

Satellite-based time series of reflected sunlight are used to determine a cloud index time series for every land surface worldwide. A satellite based daily snow cover dataset is used to aid in distinguishing snow from clouds. In addition, the global horizontal clearsky radiation G_{hc} is modeled based on the surface elevation of each location, the local time, and the measure of turbidity in the atmosphere. 3Tier opted to use a satellite-based, monthly time series of aerosol optical depth and water vapor derived from the Moderate Resolution Imaging Spectroradiometer (MODIS). This dataset was combined with another turbidity dataset that includes both surface and satellite observations to provide a turbidity measure that spans the period of our satellite dataset and is complete for all land surfaces. The cloud index n and the clear sky irradiance G_{hc} are then combined to model the global horizontal irradiance G_h. This component of the process is calibrated for each satellite based on a set of high-quality surface observations. G_h estimates are then combined with other inputs to evaluate the other irradiance components D_h and B_n.

5.4 EnMetSol

The EnMetSol method is a technique for determining the global radiation at ground by the use of data from a geostationary satellite (Beyer 1996, Hammer 2003). It is used in combination with a clear sky model to evaluate the 3 irradiance parameters G_h, D_h and B_n. The key parameter of the method is the cloud index n, which is estimated from the satellite measurements and related to the transmissivity of the atmosphere via

$$K_c = 1 - n$$

where the transmissivity is expressed by the clear sky index K_c defined as the ratio of global irradiance G_h and the corresponding clear sky irradiance G_{hc}:

$$K_c = \frac{G_h}{G_{hc}}$$

Two sets of data produced with the EnMetSol algorithm will be analyzed, corresponding to two different clear sky irradiance models:

- the model of Dumortier (Fontoynont 1998) with the Remund (2009) MeteonormHR high resolution data base for the turbidity input,

- and the original Solis clear sky model (Mueller 2004) with monthly averages of AOD (Kinne 2005) and water vapour content (Kalnay 1996) as input parameters.

For the Dumortier clearsky, a diffuse fraction model (Lorenz 2007) is used to calculate the all sky diffuse horizontal irradiance (via G_h-D_h). A recently developed beam fraction model (Hammer 2009) is used to calculate the B_n for all sky conditions with the Solis model.

5.5 IrSolAv

In the IrSolAv irradiance derivation scheme, the cloud index *n* is derived using the methodology developped by Dagestad and Olseth (Dagestad and Olseth, 2007) with some modifications in the ground albedo determination. The ground albedo is computed from a forward and backward moving window of 14 days taking into account its evolution during the day, as function of the co-scattering angle.

The global horizontal irradiance G_h is then evaluated from the cloud index with the model proposed by Zarzalejo (Zarzalejo et al., 2009); it uses as independent variables the cloud index, the 50-percentile of the cloud index for a given place, and the air mass *AM*. The normal beam irradiance B_n is calculated from the global irradiance with the help of Louche correlation (Louche et al., 1991).

In a second step, the clear sky conditions are indentified with the algorithm proposed by Polo (Polo et al., 2009a; Polo et al., 2009b); for these clear conditions, the irradiances are evaluated with the ESRA clear sky model (Rigollier 2000), using the aerosol optical depth *aod* taken from Soda, MODIS or from a method proposed by Polo (Polo et al., 2009a) depending on their availability.

6. Comparison and evaluation procedure

In terms of validation, when evaluating satellite derived parameters with the same time

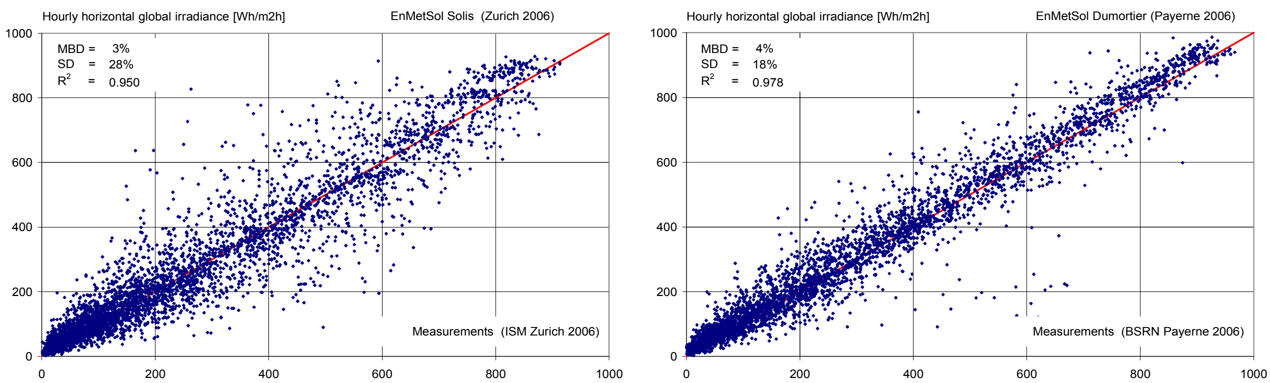

Figure 8 Scatter plots for the global horizontal irradiance produced by EnMetSol for Zurich and Payerne.

step, the comparison can be done by means of scatter plots; these give a visual evaluation of the capability of the model to reproduce the measurements. On these graphs, the diagonal line is representative of an ideal model, and the points should lay around this line. An illustration is given on Figure 8 for Zurich and Payerne, two sites that showing different dispersions.

The statistical parameters like the mean bias difference (*mbd*), the root mean square difference (*rmsd*), the standard deviation (*sd*) and the determination coefficient (R^2) represent a quantification of the model dispersion. These statistical parameters include dispersions introduced by:

- the retrieval procedure,
- the comparison of point measurements (ground data) with aera measurements,
- the comparison of the average of four instantaneous measurements with 60 minutes integrated values.

In the field of solar radiation and natural light, the comparison is often done in term of frequency of occurrence: for the irradiance, it gives an indication of the repartition for each level of radiation, and for the clearness index, that the level of radiation occures at the right time during the day. The obtained graph is a line (or a bar chart) representative of the relative frequency of occurrence of the considered parameter. This is illustrated on Figure 9 for the global irradiance and the corresponding clearness index K_t. On the same graph, the frequency of occurrence of the ground measurements are represented as grey bars, and the different models in color lines.

A second order statistic, the Kolmogorov-Smirnov test (Espinar 2009), is also applied to the data. It represents the capability of the model to reproduce the frequency of occurrence at each of the irradiance level. In order to avoid a peak at the zero level of beam irradiance, these values are excluded form the statistic. A visualisation is given on Figure 10 where the irradiance cumulated frequency of occurrence is represented against

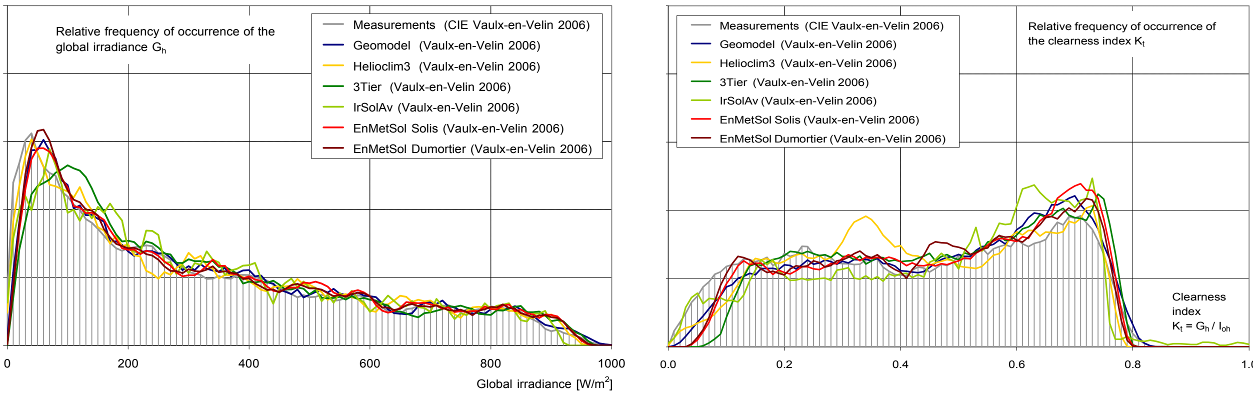

Figure 9 Global irradiance and clearness index K_t relative frequency of occurrence for data acquired in Vaulx-en-Velin (F). The grey bars are representative of the measurements.

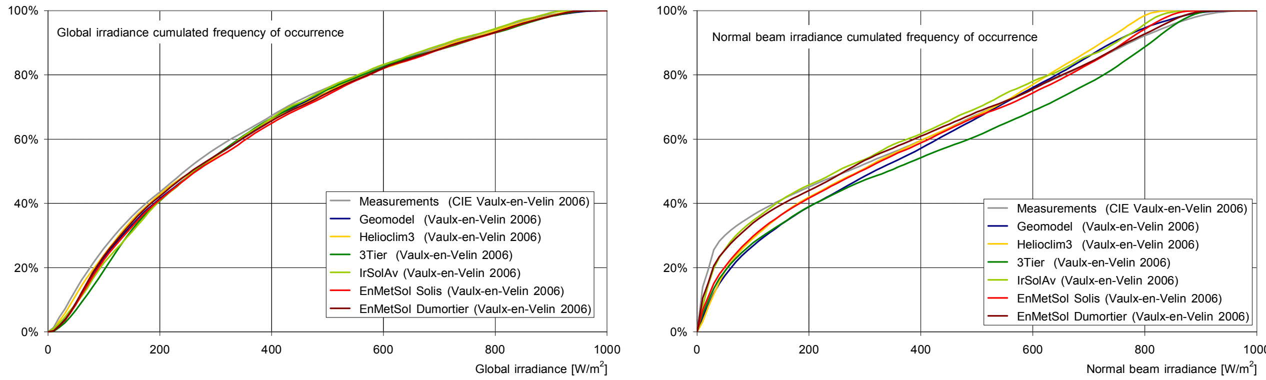

Figure 10 Relative frequency of occurrence for the global and the beam irradiance for measurements at the site of Vaulx-en-Velin.

the irradiance for the same site than above. The quantitative value representative of the Kolmogorov Smirnov test Integral (*KSI*) is defined as:

$$KSI = \int_{G_{h\min}}^{G_{h\max}} \left| F_c(G_h) - F_c(G_{h\mathrm{mod}}) \right| \cdot dG_h$$

where $F_c(G_h)$ and $F_c(G_{hmod})$ are respectively the ground measurements and the corresponding modelled cumulated frequencies of occurrence.

7. Global irradiance results

To ensure a correct and comparable validation of the different products, the following method was used to merge the products and the ground measurements: for each generated value, the nearest time stamped corresponding ground value is searched in the data base; this means that the satellite image was taken within the ground integration

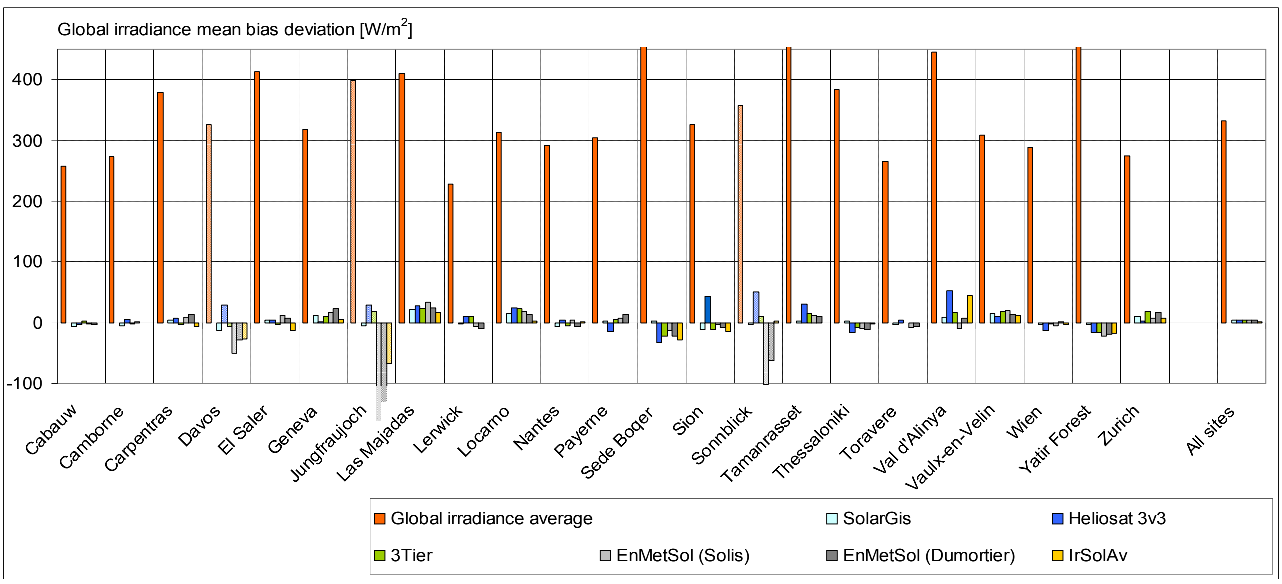

Figure 11 Average global irradiance and absolute mean bias difference

			SolarGis				Heliosat 3v3				3Tier				EnMetSol (Solis)				EnMetSol (Dumortier)				IrSolAv			
	G_h [W/m^2]	nb	R^2	mbd	sd	KSI	R^2	mbd	sd	KSI	R^2	mbd	sd	KSI	R^2	mbd	sd	KSI	R^2	mbd	sd	KSI	R^2	mbd	sd	KSI
Cabauw	258	4153	0.977	-6	49	9	0.967	-4	58	5	0.961	3	63	16	0.982	-1	43	6	0.981	-3	44	8				
Camborne	273	4087	0.976	-6	52	8	0.966	6	63	9	0.962	-2	66	15	0.981	1	47	8	0.981	0	47	8				
Carpentras	379	3993	0.985	4	48	4	0.978	7	59	10	0.980	-4	55	9	0.987	8	45	9	0.986	14	46	14	0.901	-6	121	11
Davos	326	4200	0.942	-13	89	19	0.915	29	107	31	0.915	-6	107	21	0.946	-50	89	51	0.937	-29	92	33	0.834	-28	147	34
El Saler	413	3600	0.971	4	67	6	0.971	3	67	9	0.959	-3	78	11	0.976	12	60	12	0.976	7	60	8	0.962	-13	75	19
Geneva	317	3622	0.977	12	55	12	0.974	1	59	4	0.960	10	72	12	0.983	16	47	11	0.982	22	50	22	0.943	5	86	11
Jungfraujoch	399	3311	0.899	-4	132	8	0.817	29	170	49	0.811	18	177	25	0.703	-161	208	162	0.697	-130	210	131	0.689	-67	217	67
Las Majadas	410	3509	0.976	21	62	21	0.970	28	68	28	0.966	23	73	23	0.978	34	58	34	0.979	24	57	24	0.963	16	75	16
Lerwick	228	3306	0.958	-2	59	10	0.930	11	78	18	0.920	10	80	18	0.964	-7	54	13	0.964	-10	54	14				
Locarno	314	4184	0.979	16	54	15	0.955	24	80	24	0.959	23	75	23	0.981	19	51	19	0.979	14	54	14	0.955	2	79	19
Nantes	292	4200	0.979	-7	49	9	0.948	4	79	6	0.963	-5	65	14	0.984	4	44	7	0.983	-7	45	10	0.943	1	81	9
Payerne	304	4005	0.976	3	57	4	0.964	-14	68	14	0.958	5	74	11	0.978	8	53	8	0.978	14	55	13	0.943	-1	85	16
Sede Boqer	576	2890	0.986	1	51	11	0.982	-34	57	33	0.970	-24	73	27	0.985	-15	53	18	0.986	-23	53	25	0.974	-29	70	32
Sion	325	4280	0.963	-11	75	21	0.947	43	88	43	0.954	-11	83	26	0.978	-3	58	16	0.975	-8	61	17	0.886	-14	126	33
Sonnblick	357	3933	0.858	-3	134	16	0.838	50	143	50	0.806	11	159	24	0.757	-102	159	102	0.747	-63	168	64	0.765	2	172	17
Tamanrasset	529	4293	0.985	3	56	5	0.968	30	85	30	0.970	15	80	15	0.970	11	78	14	0.972	10	76	15				
Thessaloniki	384	3675	0.982	3	53	3	0.978	-16	60	16	0.964	-8	76	16	0.975	-9	63	14	0.975	-11	64	16	0.959	-2	80	15
Toravere	266	3784	0.971	-4	53	4	0.940	3	80	16	0.944	-1	72	21	0.973	-8	51	10	0.972	-7	52	9				
Val d'Alinya	446	2499	0.968	9	76	11	0.927	52	117	52	0.951	17	94	17	0.965	-10	80	23	0.966	7	78	17	0.927	45	116	45
Vaulx-en-Velin	308	4141	0.980	15	51	14	0.972	11	60	11	0.965	18	66	18	0.983	19	46	19	0.983	14	47	14	0.950	11	79	13
Wien	288	4203	0.973	-3	55	6	0.969	-13	61	13	0.963	-2	64	13	0.981	-5	47	7	0.981	1	47	3	0.932	-3	87	11
Yatir Forest	549	3221	0.984	-4	53	7	0.980	-16	59	18	0.974	-16	66	17	0.988	-22	47	23	0.987	-20	47	21	0.972	-18	69	18
Zurich	274	4192	0.953	10	74	12	0.940	3	87	13	0.937	18	85	19	0.950	8	76	9	0.950	16	79	16	0.920	7	95	10
All sites	332	75837	n/a	3	55	n/a	n/a	4	70	n/a	n/a	4	70	n/a	n/a	4	54	n/a	n/a	4	55	n/a	n/a	1	83	n/a

Table II First and second order statistics in absolute values for the global horizontal irradiance. The sites in grey are not taken into account in the overall statistics.

			SolarGis				Heliosat 3v3				3Tier				EnMetSol (Solis)				EnMetSol (Dumortier)				IrSolAv			
	G_h [W/m^2]	nb	R^2	mbd%	sd%	KSI	R^2	mbd%	sd%	KSI	R^2	mbd%	sd%	KSI	R^2	mbd%	sd%	KSI	R^2	mbd%	sd%	KSI	R^2	mbd%	sd%	KSI
Cabauw	258	4153	0.977	-3	19	9	0.967	-2	23	5	0.961	1	24	16	0.982	-1	17	6	0.981	-1	17	8				
Camborne	273	4087	0.976	-2	19	8	0.966	2	23	9	0.962	-1	24	15	0.981	1	17	8	0.981	0	17	8				
Carpentras	379	3993	0.985	1	13	4	0.978	2	16	10	0.980	-1	14	9	0.987	2	12	9	0.986	4	12	14	0.901	-2	32	11
Davos	326	4200	0.942	-4	27	19	0.915	9	33	31	0.915	-2	33	21	0.946	-15	27	51	0.937	-9	28	33	0.834	-8	45	34
El Saler	413	3600	0.971	1	16	6	0.971	1	16	9	0.959	-1	19	11	0.976	3	14	12	0.976	2	14	8	0.962	-3	18	19
Geneva	317	3622	0.977	4	17	12	0.974	0	19	4	0.960	3	23	12	0.983	5	15	11	0.982	7	16	22	0.943	2	27	11
Jungfraujoch	399	3311	0.899	-1	33	8	0.817	7	43	49	0.811	5	44	25	0.703	-40	52	162	0.697	-33	53	131	0.689	-17	54	67
Las Majadas	410	3509	0.976	5	15	21	0.970	7	17	28	0.966	6	18	23	0.978	8	14	34	0.979	6	14	24	0.963	4	18	16
Lerwick	228	3306	0.958	-1	26	10	0.930	5	34	18	0.920	4	35	18	0.964	-3	24	13	0.964	-4	24	14				
Locarno	314	4184	0.979	5	17	15	0.955	8	25	24	0.959	7	24	23	0.981	6	16	19	0.979	4	17	14	0.955	1	25	19
Nantes	292	4200	0.979	-2	17	9	0.948	1	27	6	0.963	-2	22	14	0.984	1	15	7	0.983	-2	16	10	0.943	0	28	9
Payerne	304	4005	0.976	1	19	4	0.964	-5	23	14	0.958	2	24	11	0.978	3	17	8	0.978	4	18	13	0.943	0	28	16
Sede Boqer	576	2890	0.986	0	9	11	0.982	-6	10	33	0.970	-4	13	27	0.985	-3	9	18	0.986	-4	9	25	0.974	-5	12	32
Sion	325	4280	0.963	-3	23	21	0.947	13	27	43	0.954	-3	25	26	0.978	-1	18	16	0.975	-2	19	17	0.886	-4	39	33
Sonnblick	357	3933	0.858	-1	38	16	0.838	14	40	50	0.806	3	44	24	0.757	-29	45	102	0.747	-18	47	64	0.765	1	48	17
Tamanrasset	529	4293	0.985	0	11	5	0.968	6	16	30	0.970	3	15	15	0.970	2	15	14	0.972	2	14	15				
Thessaloniki	384	3675	0.982	1	14	3	0.978	-4	16	16	0.964	-2	20	16	0.975	-2	16	14	0.975	-3	17	16	0.959	-1	21	15
Toravere	266	3784	0.971	-1	20	4	0.940	1	30	16	0.944	0	27	21	0.973	-3	19	10	0.972	-3	20	9				
Val d'Alinya	446	2499	0.968	2	17	11	0.927	12	26	52	0.951	4	21	17	0.965	-2	18	23	0.966	2	18	17	0.927	10	26	45
Vaulx-en-Velin	308	4141	0.980	5	16	14	0.972	3	20	11	0.965	6	22	18	0.983	6	15	19	0.983	5	15	14	0.950	4	26	13
Wien	288	4203	0.973	-1	19	6	0.969	-4	21	13	0.963	-1	22	13	0.981	-2	16	7	0.981	0	16	3	0.932	-1	30	11
Yatir Forest	549	3221	0.984	-1	10	7	0.980	-3	11	18	0.974	-3	12	17	0.988	-4	9	23	0.987	-4	9	21	0.972	-3	13	18
Zurich	274	4192	0.953	4	27	12	0.940	1	32	13	0.937	6	31	19	0.950	3	28	9	0.950	6	29	16	0.920	3	35	10
All sites	332	75837	n/a	1	17	n/a	n/a	1	21	n/a	n/a	1	21	n/a	n/a	1	16	n/a	n/a	1	16	n/a	n/a	0	33	n/a

Table III First and second order statistics in relative values for the global horizontal irradiance. The sites in grey are not taken into account in the overall statistics.

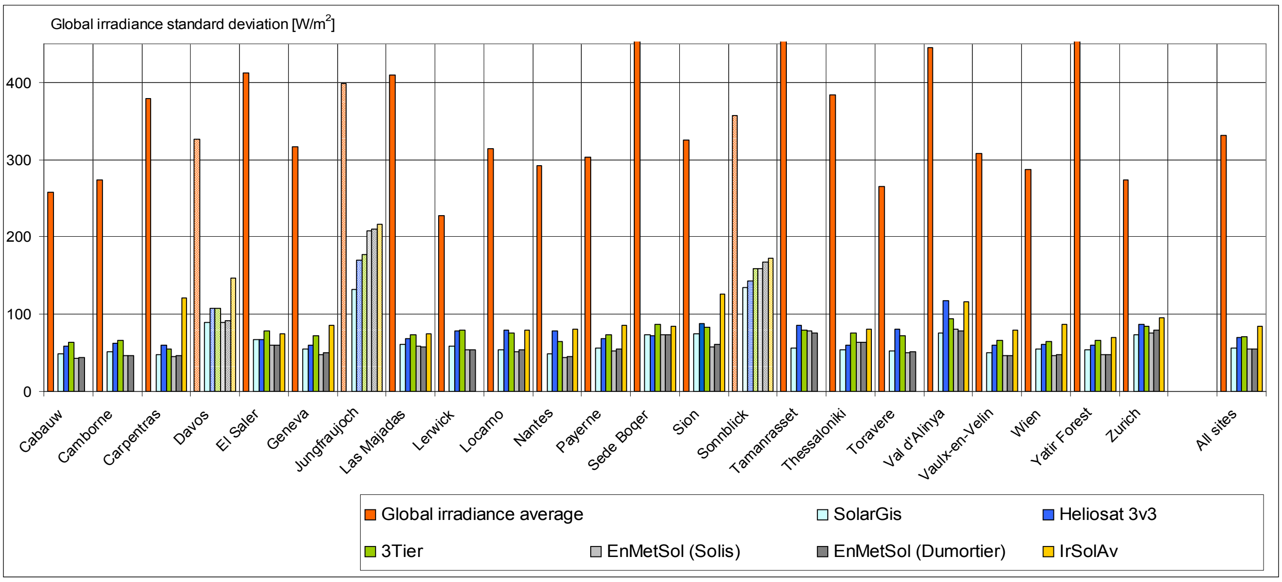

Figure 12 Absolute standard deviation for the global irradiance. In red, the average G_h.

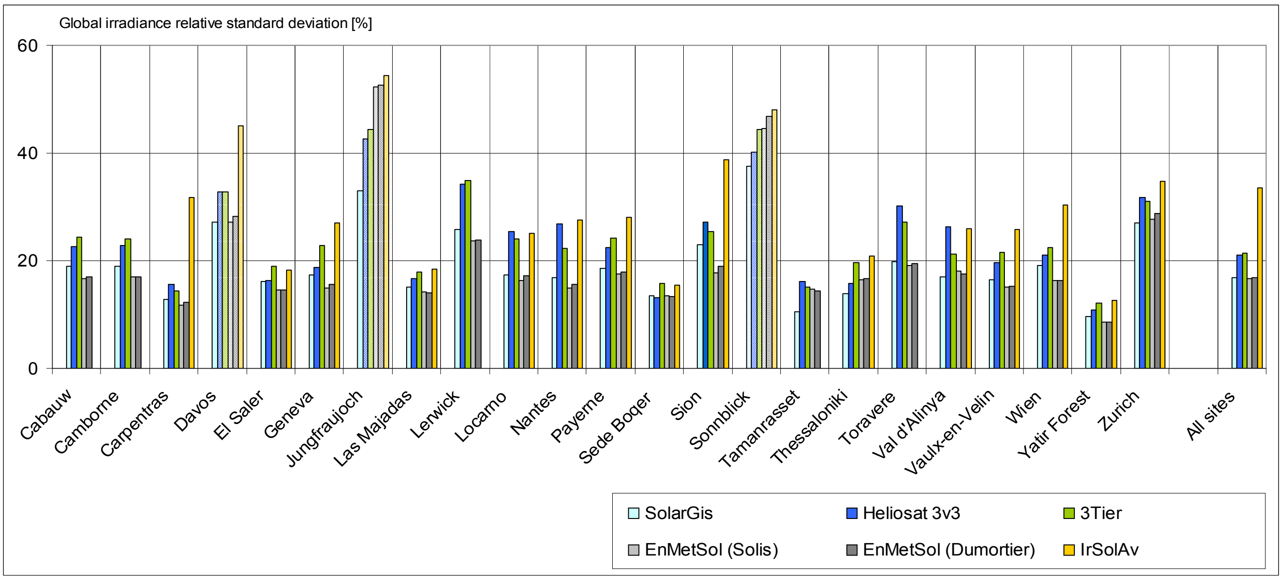

Figure 13 Relative standard deviation for the global irradiance.

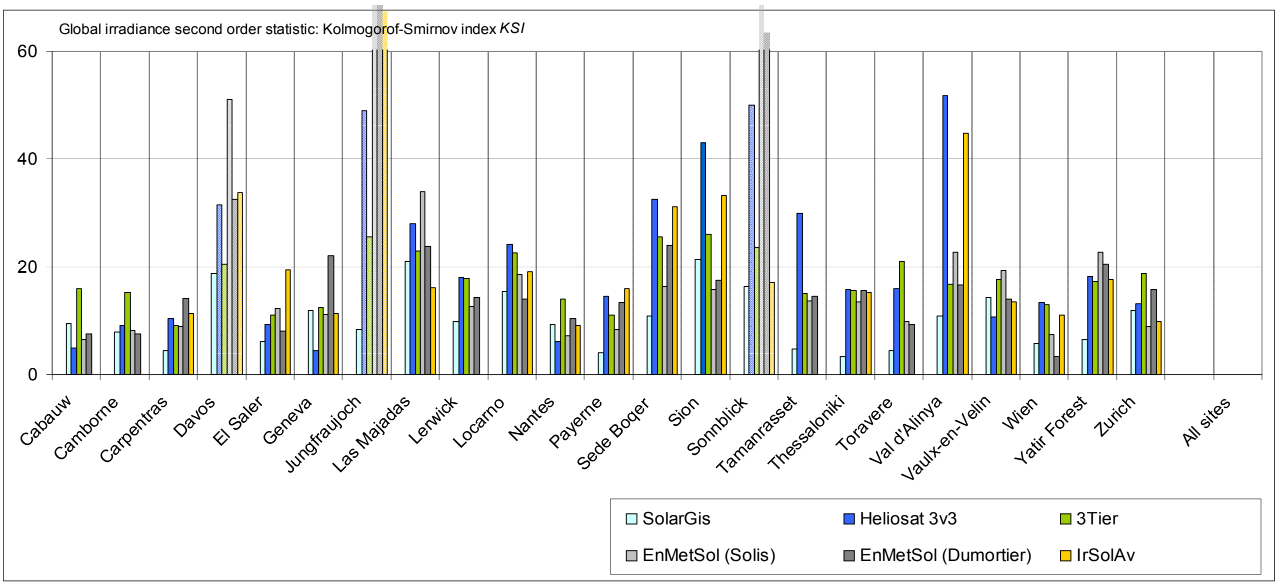

Figure 14 Second order statistics *KSI* for the global irradiance

period. Then, only hours for which ground and both generated products are present are taken into account in the validation procedure; so, mainly the ground data availability restrict the number of points in the comparison.

The results of the validation are given on Table II and Table III respectively in absolute and relative values. The corresponding graphs are given on Figure 11 to 14.

The first established fact is that the sites of Davos, Jungfraujoch and Sonnblick give much higher differences than the other stations. This is due to the snow cover during all or part of the year, which is not taken into account by all the models, and is difficult to evaluate precisely. This is clearly visible on frequency of occurrence plotted fir the clearness index as shown on Figure 15 for the site of Sonnblick. These site are not part of the overall statistics. The site of Nantes is also represented on Figure 15 for comparison purpose.

The overall average mean bias deviation is very low for all the products, and except for heliosat 3, the sign of the mean bias deviation is in general the same for all the algorithms. It is interesting to note that for high latitude sites (Cabauw, Camborne, Lerwick and Toravere), the bias is even lower than for the middle latitude sites. The site of Val d'Alynia in Spain shows slightly variable bias depending on the product, this can be explained by

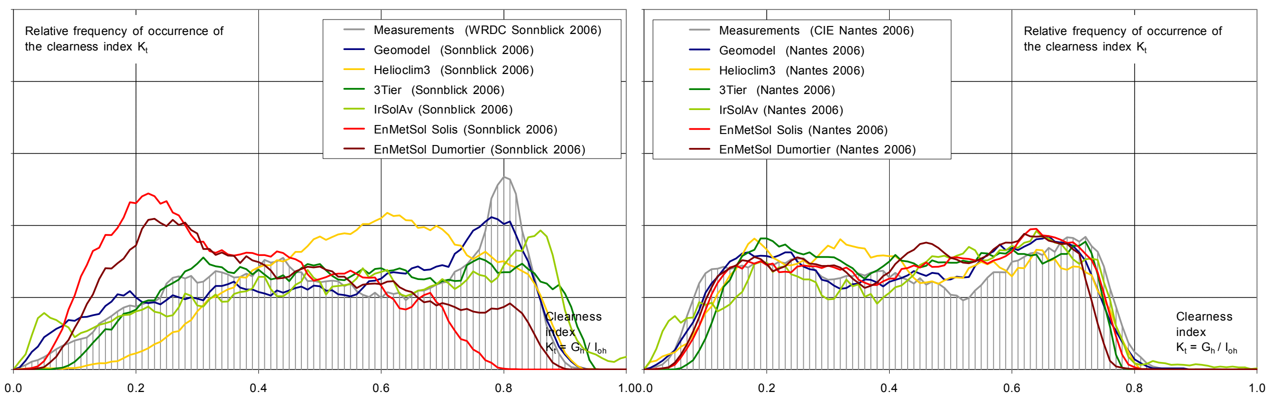

Figure 15 Frequency of occurence of the clearness index for the site of Sonneblick (high altitude and snow) and for Nantes.

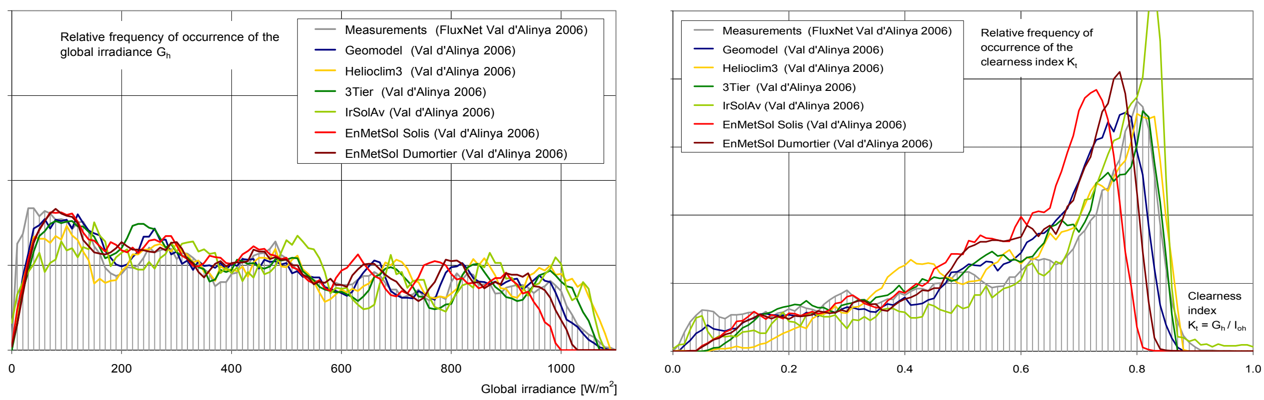

Figure 16 Frequency of occurence of global irradiance and the clearness index for the site of Val d'Alynia.

the high altitude of the site (1770m) and the mountainous environment. The produced irradiance varie from one algorithm to the other; the corresponding graph is given on Figure 16 for the global irradiance and the clearness index. This can be due to the clear sky model used for the normalisation in conjunction with their input parameter (atmospheric water vapor content, aerosol load and linke turbidity).

In term of absolute standard deviation (due to the negligible bias, the root mean square difference and the standard deviation are equivalent), except for the high altitude stations (Davos, Jungfraujoch, Sonnblick and Val d'Alynia), all the site show the same order of magnitude, including the high latitude sites. Due to the high irradiance level for Carpentras, Sede Boqer, Tamanrasset and Yatir forest, the sites show good relative standard deviations.

The choice of a clear sky model is a key point in the satellite irradiance derivation, it will have a direct influence on the output. The measured and modelled global clearness

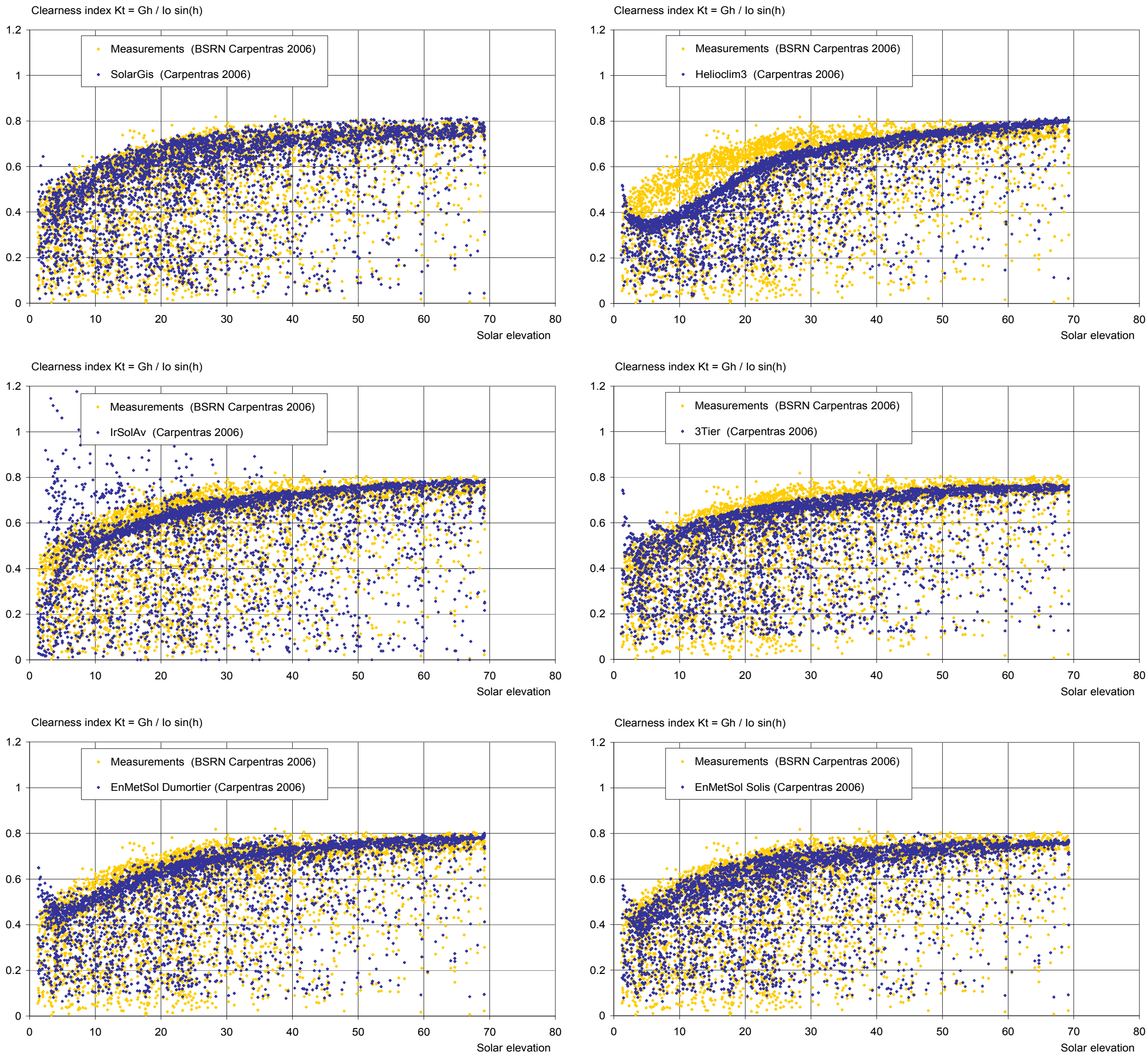

Figure 17 The global clearness index K_t represented against the solar elevation angle for the site of Carpentras. In yellow, the measurements and in blue the different products.

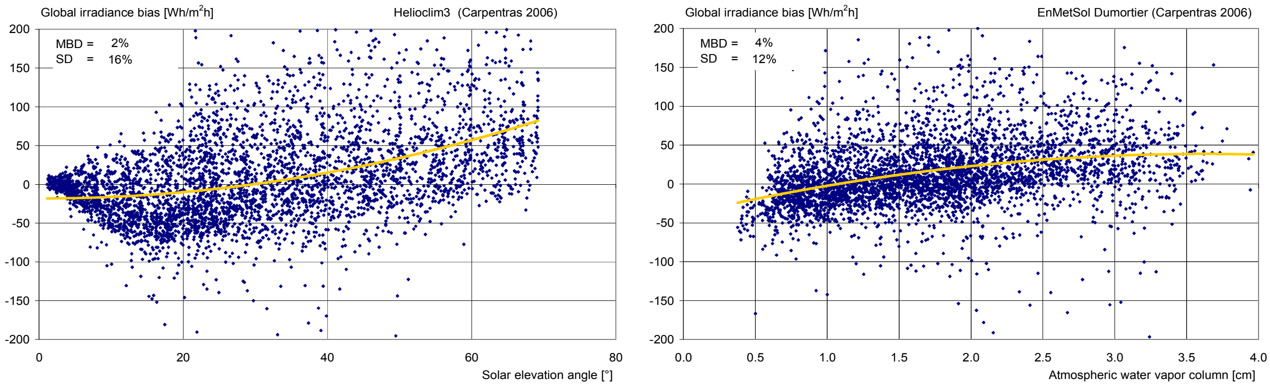

Figure 18 Global irradiance mean bias difference against the solar elevation angle (left) and the atmospheric water vapor content for two products and the site of Carpentras.

index is plotted against the solar elevation for all the products and the site of Carpentras on Figure 17. On these graphs, the clear sky conditions are represented by the upper boundary; it is interesting to point out that even if there is a great gap between the measurements and the modelled values for Helioclim, the overall performance is of the same order of magnitude than for the other products. It can also be noted here that for half of the products, the highest and the lowest modelled values of K_t are never reached.

To better understand the bias, a dependence analysis is done with the solar elevation angle and the water vapor column. To illustrate the results, two examples are given on Figure 18 where the bias is represented against the considered parameter, and a best fit is traced to underline the tendency. If the main pattern of all the models is to underestimate the global irradiance for low water vapor column values and overestimate it for high w, the bias pattern is variable from one model to the other with the solar elevation angle.

The study was also done with the turbidity, but this parameter was not available except for the sites of Carpentras and Sede Boqer, and on a daily basis. As for the water vapor content, the general tendency is a positive slope on the bias with the daily aerosol optical depth. An illustration for EnMetSol is given on Figure 19.

The irradiance for clear sky conditions is directly derived from the clear sky model. For

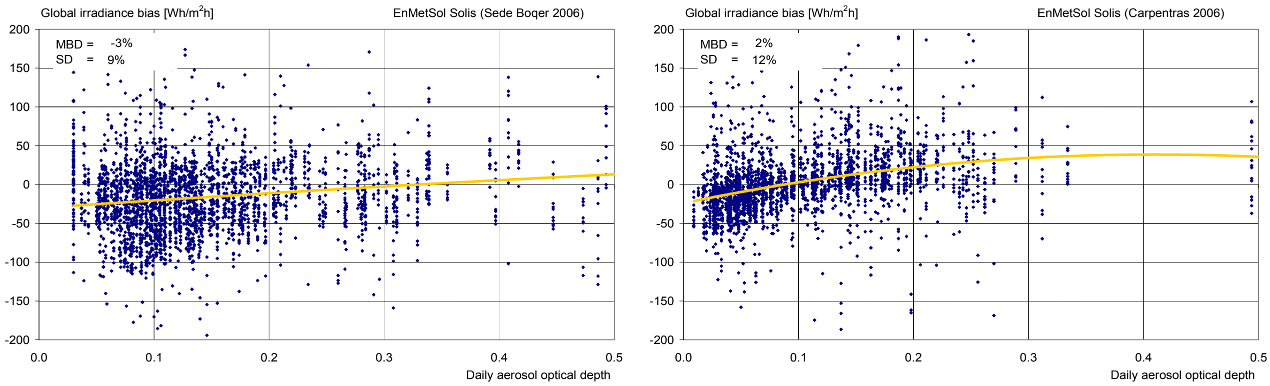

Figure 19 Global irradiance mean bias difference against the daily aerosol load of the atmosphere for the two sites of Sede Boqer and Carpentras.

			SolarGis		Heliosat 3v3		3Tier		EnMetSol (Solis)		EnMetSol (Dumortier)		IrSolAv	
sky type	G_h	nb	mbd	sd	mbd	sd	mbd	sd	mbd	sd	mbd	sd	mbd	sd
clear	498	35824	-9	43	-23	49	-18	57	-16	41	-16	43	-25	66
			-2%	9%	-5%	10%	-4%	11%	-3%	8%	-3%	9%	-7%	17%
intermediate	249	24096	12	67	22	75	12	80	20	60	19	61	19	95
			5%	27%	9%	30%	5%	32%	8%	24%	8%	25%	11%	53%
overcast	82	15917	18	49	39	65	42	62	25	48	24	48	36	79
			22%	60%	48%	80%	51%	75%	30%	58%	29%	59%	63%	138%

Table IV First order statistics in absolute and relative values for the global horizontal irradiance and for the three sky conditions. The absolute values are in [W/m²].

all sky condition, the clear sky model is combined with the cloud index. It is therefore interesting to differentiate the sky conditions following the rules defined in section 4. Table IV gives the overall results obtained for the three sky types. Without surprise, the clear sky conditions show the lowest standard deviation. All the algorithms have the same tendency to underestimate for clear conditions, and overestimate the global irradiance for intermediate and overcast conditions. Going more into details, the same tendency is also visible for all the sites. This is illustrated on Figure 20 for a cloudy (Lerwick) and a sunny (Carpentras) site. All the Figures and the complete Tables are given in the Annex.

The second order statistic given by the Kolmogorov-Smirnov index is a combination of

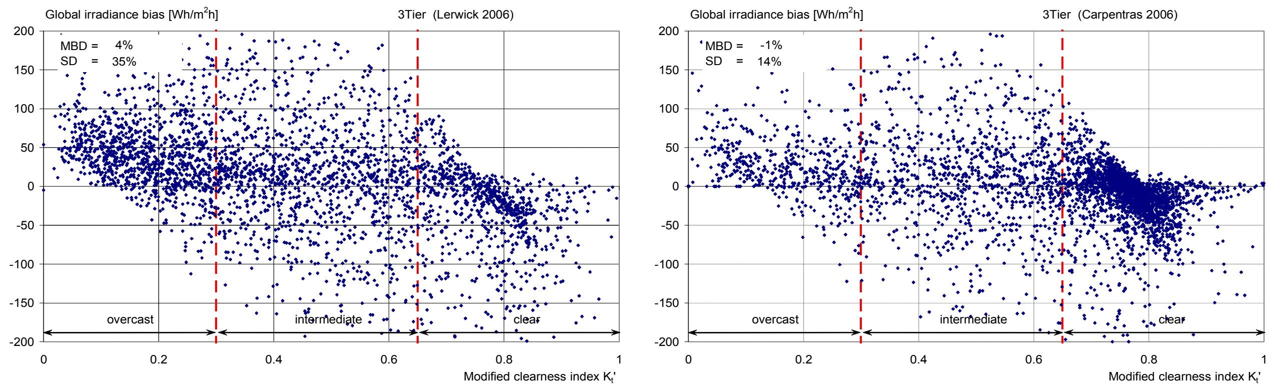

Figure 20 Global irradiance mean bias difference against the modified clearness index for the two sites of Lerwick and Carpentras.

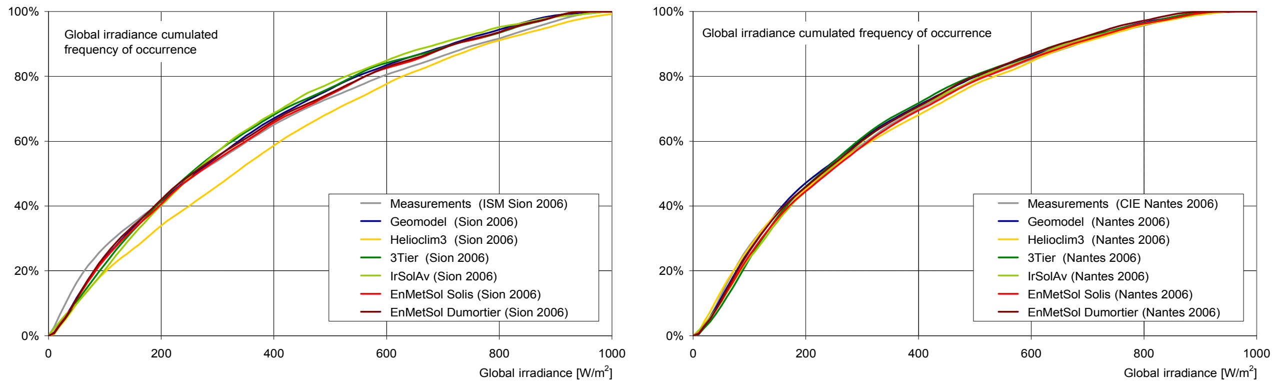

Figure 21 Clearness index cumulated frequecy of occurrence for two sites with comparable standard deviation: Sion and Nantes.

the bias, the standard deviation (dispersion) and the cumulated frequency of occurence. It is more sensitive and highlights smaller deviations than the first order indicators. This can be seen for example for the sites of Sion or Sede Boqer, where the standard deviation is similar to the other sites, but the clearness index frequency of occurence shows descreapancies with the corresponding measurements. The cumulated frequency of occurrence for Sion and Nantes are given on Figure 21. The deviation from the measurements in Sion is visible for all the models at low and high irradiance levels; it can be due to snow in the Rhône Valley.

In conclusion, except for the four high altitude sites (potentially with snow), the average bias is around 1% (4 [W/m^2]), positive for all the models. The best product derives the global irradiance with a standard deviation of 16% (55 [W/m^2]).

Some models never reach the measured highest and lowest clearness index. The majority of the products show a bias dependance with the solar elevation angle, the water vapor column and when available, with the aerosol optical depth. In term of sky type, the general pattern is to underestimate the global irradiance for clear conditions, and to overestimate it for all the other conditions. Not all models take into account the snow, but even when included in the algorithm, the global irradiance for the concerned sites is not satisfactory.

8. Beam irradiance results

The same methodology is used for the validation of the beam irradiance component, except that the slots with no direct irradiance are excluded from the validation in order to avoid a bias in the overall statistic and a peak at zero irradiance in the frequency of occurrence.

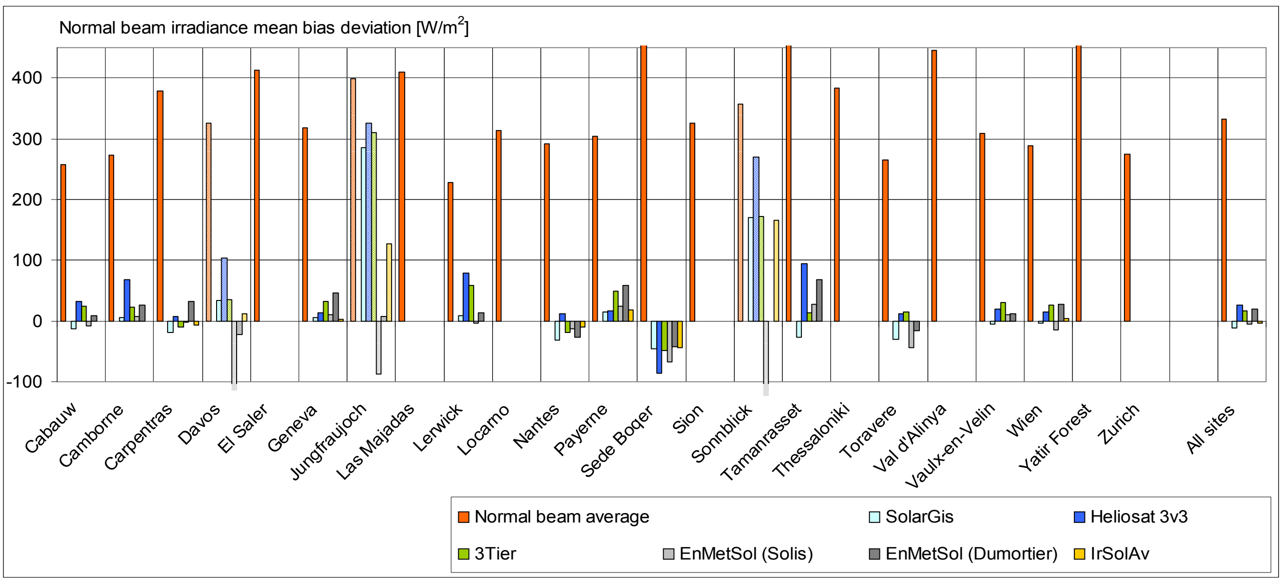

Figure 22 Average beam irradiance and absolute mean bias difference

			SolarGis				Heliosat 3v3				3Tier				EnMetSol (Solis)				EnMetSol (Dumortier)				IrSolAv			
	B_n [W/m^2]	nb	R^2	mbd	sd	KSI	R^2	mbd	sd	KSI	R^2	mbd	sd	KSI	R^2	mbd	sd	KSI	R^2	mbd	sd	KSI	R^2	mbd	sd	KSI
Cabauw	220	4095	0.939	-13	93	28	0.877	32	130	28	0.868	24	136	14	0.931	-8	100	47	0.933	10	97	39				
Camborne	231	3471	0.942	6	96	28	0.885	68	134	26	0.896	22	129	20	0.937	7	101	46	0.940	27	98	31				
Carpentras	448	3993	0.936	-19	118	45	0.856	8	172	37	0.905	-9	141	30	0.924	-3	129	39	0.923	32	128	20	0.729	-6	237	28
Davos	314	4200	0.864	34	187	94	0.748	104	247	108	0.707	35	271	113	0.735	-115	257	276	0.757	-23	244	190	0.663	12	291	153
El Saler																										
Geneva	307	3622	0.918	5	125	41	0.887	13	145	39	0.869	32	161	42	0.933	10	113	35	0.937	46	112	14	0.853	3	165	34
Jungfraujoch	185	3311	0.541	285	360	158	0.327	326	373	216	0.461	310	381	174	0.319	-88	350	578	0.333	7	365	485	0.399	127	365	365
Las Majadas																										
Lerwick	157	3119	0.890	9	110	30	0.782	78	160	42	0.764	58	168	47	0.902	-4	104	41	0.906	13	102	27				
Locarno																										
Nantes	284	4199	0.943	-31	95	37	0.838	12	157	32	0.890	-19	132	25	0.945	-14	94	27	0.944	-27	96	33	0.851	-9	154	11
Payerne	264	4005	0.889	15	140	32	0.841	16	166	73	0.832	49	178	12	0.887	24	142	48	0.893	58	142	30	0.821	19	177	68
Sede Boqer	638	2746	0.887	-46	115	56	0.763	-86	168	101	0.760	-49	166	63	0.835	-68	138	84	0.826	-43	144	62	0.700	-43	187	60
Sion																										
Sonnblick	257	3933	0.708	171	276	32	0.496	270	334	80	0.487	173	363	58	0.455	-123	320	365	0.450	0	346	246	0.524	166	359	85
Tamanrasset	545	4293	0.927	-27	138	61	0.756	94	235	82	0.811	14	208	62	0.819	27	204	60	0.843	68	191	71				
Thessaloniki																										
Toravere	286	3784	0.929	-30	112	36	0.807	13	183	47	0.792	15	188	32	0.890	-43	140	84	0.897	-15	133	65				
Val d'Alinya																										
Vaulx-en-Velin	316	4060	0.939	-6	103	34	0.888	19	137	30	0.893	30	140	54	0.946	11	96	23	0.950	12	94	11	0.878	0	144	21
Wien	257	4203	0.900	-3	124	92	0.880	15	135	129	0.858	26	150	84	0.907	-15	121	143	0.909	27	119	116	0.834	3	158	140
Yatir Forest																										
Zurich																										
All sites	326	45590	n/a	-11	115	n/a	n/a	25	163	n/a	n/a	17	160	n/a	n/a	-5	128	n/a	n/a	19	125	n/a	n/a	-3	176	n/a

Table V First and second order statistics in absolute values for the normal beam irradiance. The sites in grey are not taken into account in the overall statistics.

			SolarGis				Heliosat 3v3				3Tier				EnMetSol (Solis)				EnMetSol (Dumortier)				IrSolAv			
	B_n [W/m^2]	nb	R^2	mbd%	sd%	KSI	R^2	mbd%	sd%	KSI	R^2	mbd%	sd%	KSI	R^2	mbd%	sd%	KSI	R^2	mbd%	sd%	KSI	R^2	mbd%	sd%	KSI
Cabauw	220	4095	0.939	-6	42	28	0.877	15	59	28	0.868	11	62	14	0.931	-4	45	47	0.933	4	44	39				
Camborne	231	3471	0.942	3	42	28	0.885	29	58	26	0.896	10	56	20	0.937	3	44	46	0.940	12	42	31				
Carpentras	448	3993	0.936	-4	26	45	0.856	2	38	37	0.905	-2	32	30	0.924	-1	29	39	0.923	7	29	20	0.729	-1	53	28
Davos	314	4200	0.864	11	60	94	0.748	33	79	108	0.707	11	86	113	0.735	-36	82	276	0.757	-7	78	190	0.663	4	92	153
El Saler																										
Geneva	307	3622	0.918	2	41	41	0.887	4	47	39	0.869	10	52	42	0.933	3	37	35	0.937	15	36	14	0.853	1	54	34
Jungfraujoch	185	3311	0.541	154	194	158	0.327	176	201	216	0.461	167	206	174	0.319	-48	189	578	0.333	4	197	485	0.399	69	197	365
Las Majadas																										
Lerwick	157	3119	0.890	6	70	30	0.782	50	102	42	0.764	37	107	47	0.902	-2	67	41	0.906	8	65	27				
Locarno																										
Nantes	284	4199	0.943	-11	34	37	0.838	4	55	32	0.890	-7	46	25	0.945	-5	33	27	0.944	-9	34	33	0.851	-3	54	11
Payerne	264	4005	0.889	6	53	32	0.841	6	63	73	0.832	19	67	12	0.887	9	54	48	0.893	22	54	30	0.821	7	67	68
Sede Boqer	638	2746	0.887	-7	18	56	0.763	-13	26	101	0.760	-8	26	63	0.835	-11	22	84	0.826	-7	23	62	0.700	-7	29	60
Sion																										
Sonnblick	257	3933	0.708	66	107	32	0.496	105	130	80	0.487	67	141	58	0.455	-48	125	365	0.450	0	135	246	0.524	65	140	85
Tamanrasset	545	4293	0.927	-5	25	61	0.756	17	43	82	0.811	2	38	62	0.819	5	37	60	0.843	13	35	71				
Thessaloniki																										
Toravere	286	3784	0.929	-11	39	36	0.807	4	64	47	0.792	5	66	32	0.890	-15	49	84	0.897	-5	47	65				
Val d'Alinya																										
Vaulx-en-Velin	316	4060	0.939	-2	33	34	0.888	6	43	30	0.893	10	44	54	0.946	3	31	23	0.950	4	30	11	0.878	0	46	21
Wien	257	4203	0.900	-1	48	92	0.880	6	53	129	0.858	10	58	84	0.907	-6	47	143	0.909	11	46	116	0.834	1	62	140
Yatir Forest																										
Zurich																										
All sites	326	45590	n/a	-4	35	n/a	n/a	8	50	n/a	n/a	5	49	n/a	n/a	-1	39	n/a	n/a	6	38	n/a	n/a	-1	54	n/a

Table VI First and second order statistics in relative values for the normal beam irradiance. The sites in grey are not taken into account in the overall statistics.

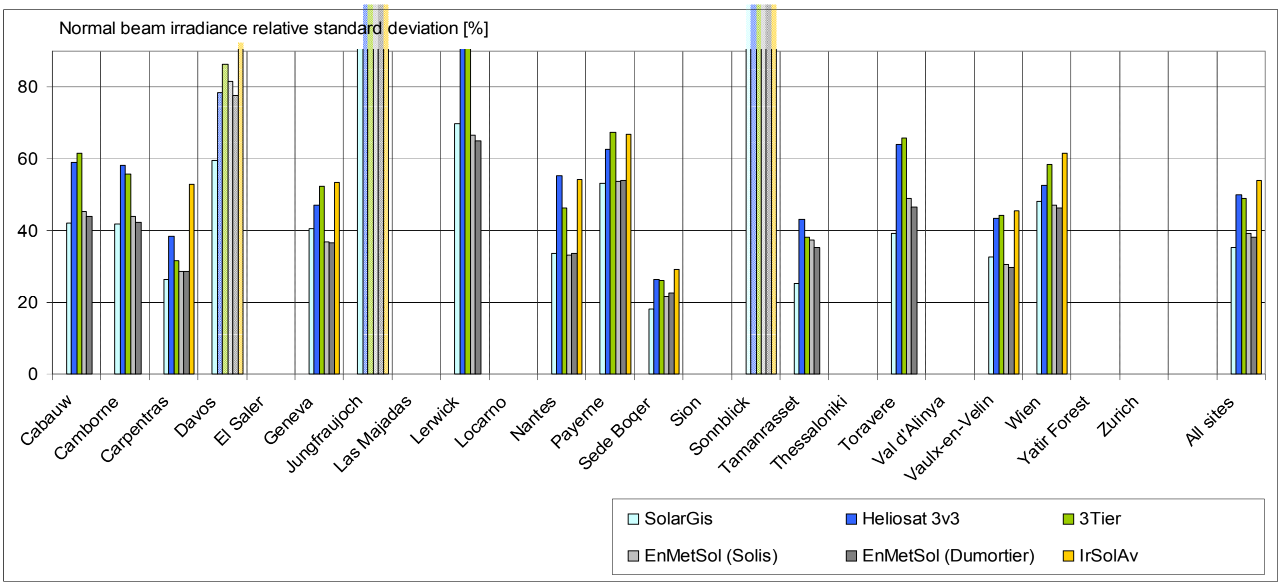

Figure 23 Relative standard deviation for the global irradiance.

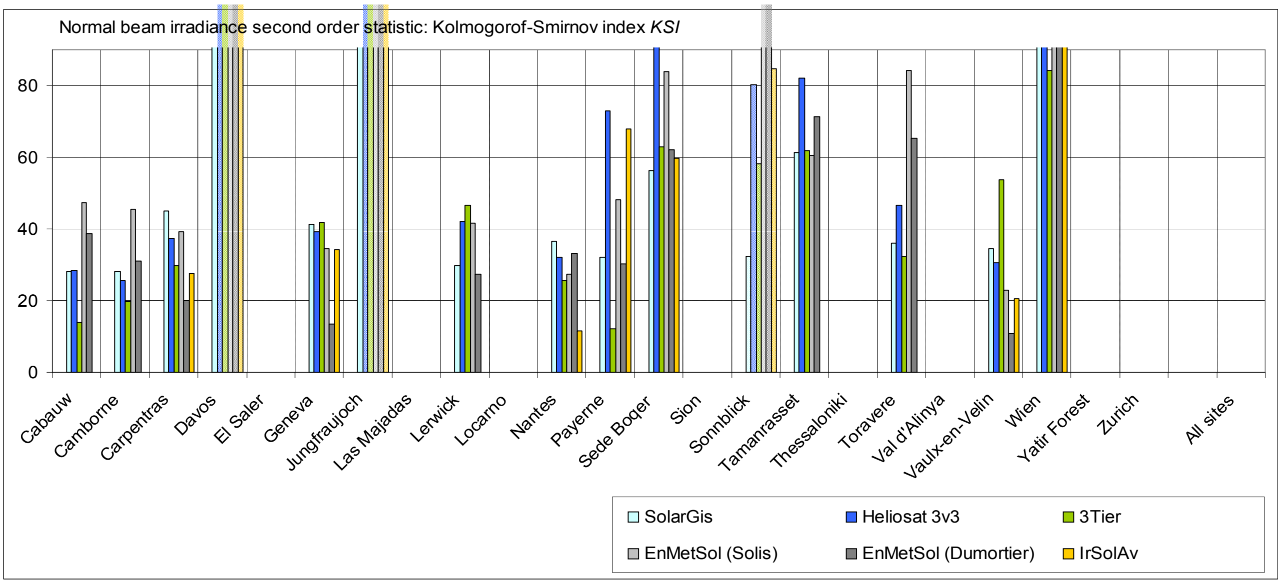

Figure 24 Second order statistics *KSI* for the global irradiance

The first and second statistics are given on Table V and VI, and on Figures 22 to 24. It can be seen on Figure 22 that the absolute bias for the beam component is variable from one site to the other, and depends on the product: for example, it is positive in Payerne (15-60 W/m2) and highly negative in Sede Boqer (-70 to -110 W/m2). For Tamanrasset, it varies from -27 [W/m^2] (Geomodel) to +68 [W/m^2] (EnMetSol) and +94 [W/m^2] (Heliosat), and for Lerwick, from -4 to +78 [W/m^2].

The standard deviation varies from 20% to 100%; it is highly variable in absolute and relative values. The site of Sede Boqer show the best values, but as it is a standard deviation, it doesn't take into account the its high mean bias. These deviation are illustrated on Figure 25, where on the left graph, the beam clearness index K_b is represented versus the solar elevation angle. It can be seen that the modelled clear sky upper limit never reaches the corresponding measurements. On the right graph, the

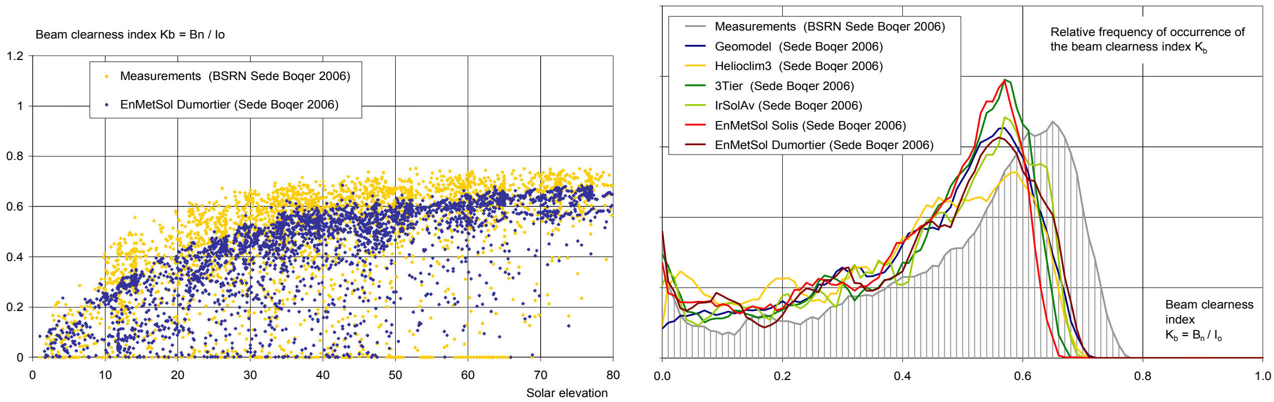

Figure 25 Beam clearness index versus the solar elevation angle, and the corresponding relative frequency of occurrence for the site of Sede Boqer.

frequency of occurrence is represented: the clear sky peak is to low for all the products. Part of the discreapancy can be an calibration issue. In fact, when comparing the BSRN beam ground measurements with the clear sky irradiance evaluated with solis from aeronet *aod* measurements, a 4% difference is visible as illustrated on Figure 26 (left: uncorrected, right: corrected by 4%). Also, inspecting BSRN data from Sede Boqer, a common 41 days sequence was found in data from 2005 and 2006. Comparison with satellite evaluated data conducted to eliminate this sequence from the present validation as it was much better reproduced with 2005 data. The 4% correction is allready included in the above results.

The relative standard deviation is comparable for all the sites, except for Lerwick, the

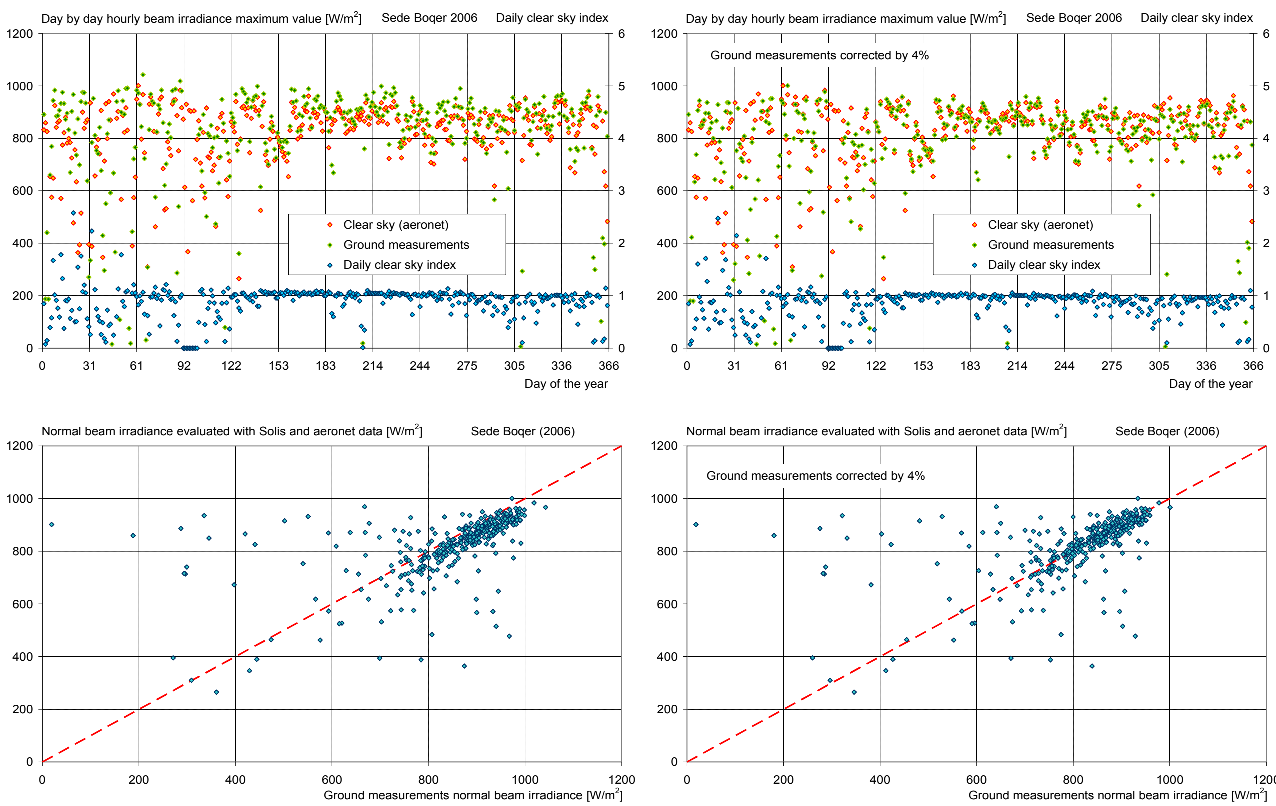

Figure 26 Sede Boqer beam irradiance before and after correction. On top, beam irradiance and clear sky index; bottom, daily measurements and évaluated data.

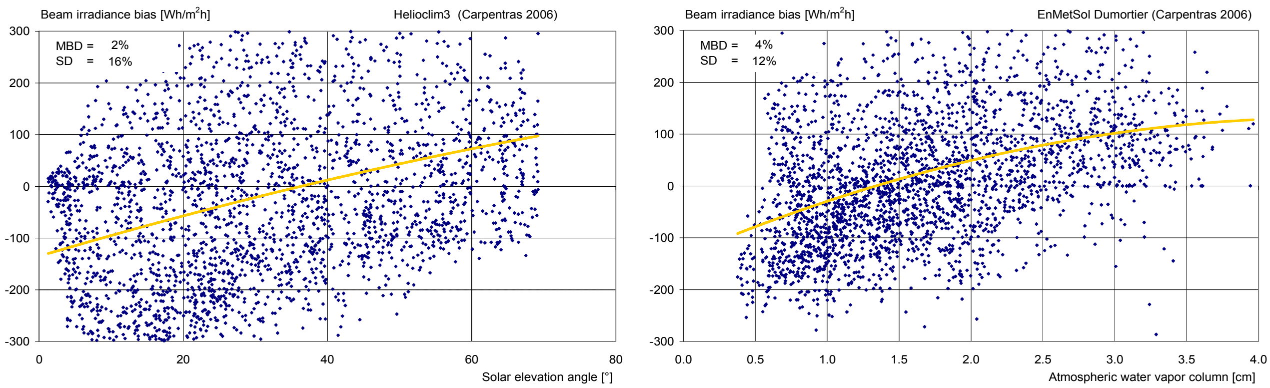

Figure 27 Normal beam irradiance mean bias difference against the solar elevation angle (left) and the atmospheric water vapor content (right) for the site of Carpentras.

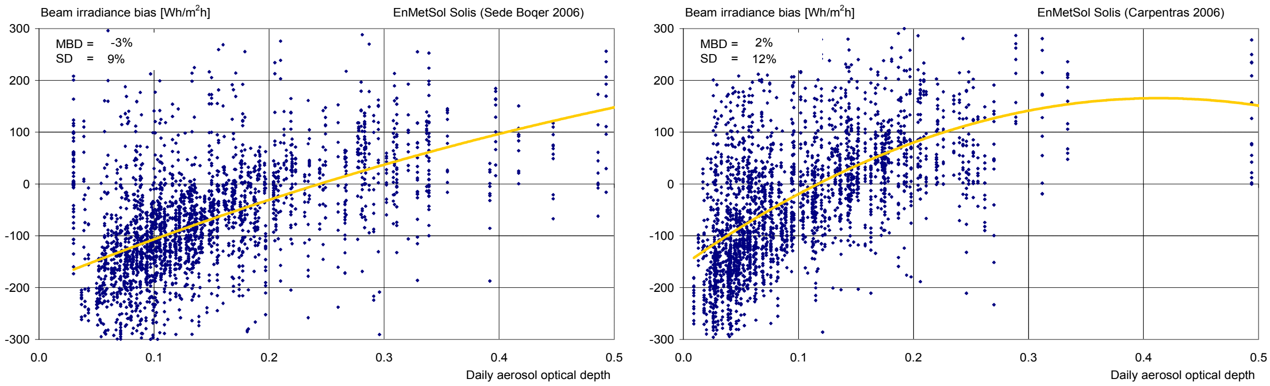

Figure 28 Normal beam irradiance mean bias difference against the daily aerosol load of the atmosphere for the two sites of Sede Boqer and Carpentras.

highest site in term of latitude, and where the average beam irradiance is very low. As for the global component, the results are good for the high latitude sites, and, due to the snow, not significative for the high altitude sites.

The same parameter dependance than for the global irradiance is conducted on the beam component. The results are given on Figures 27 and 28, where the same sites and models as for the global component are represented; they show very similar pattern (see Figures 18 and 19). This is a consequence of the method used to derive the beam irradiance: all the algorithm derive in a first step the global component, and split it into beam and diffuse with the help of a diffuse fraction model (Dirindex (Perez 1992) for SolarGis, Liu and Jordan (Liu 1960) for Helioclim, and in-house models for the other products). This means that the conclusion drawn for the global are also valid for the

			SolarGis		**Heliosat 3v3**		**3Tier**		**EnMetSol (Solis)**		**EnMetSol (Dumortier)**		**IrSolAv**	
sky type	B_n	nb	mbd	sd	mbd	sd	mbd	sd	mbd	sd	mbd	sd	mbd	sd
clear	627	20352	-66	121	-61	163	-45	161	-66	138	-24	137	-83	179
			-10%	19%	-10%	26%	-7%	26%	-10%	22%	-4%	22%	-13%	29%
intermediate	142	15173	40	110	119	146	81	163	58	108	72	114	73	171
			28%	78%	84%	103%	57%	115%	41%	76%	51%	81%	52%	120%
overcast	5	10065	14	45	51	70	38	93	18	50	18	52	39	89
			302%	983%	1117%	1522%	831%	2022%	394%	1084%	393%	1129%	845%	1927%

Table VII First order statistics in absolute and relative values for the normal beam irradiance and for the three sky conditions. The absolute values are in [W/m^2].

beam irradiance, even if the effects are more important due to the chained models.

The validation results for the three categories of the sky type are given on Table VII where the results for overcast conditions are included, even if they are not significative. Here again, comparable conclusions can be drawn, the bias is negative for clear conditions and positive for intermediate skies.

The above results are also visible on the second order statistic *KSI*, as illustrated on Figure 24 and 29, and given in Table V and VI. The fact that the beam is measured or retrieved from the global and the diffuse is not the main issue on the difference in the cumulated frequency of occurrence curves, it is more a site effect.

In conclusion, the beam irradiance is retrieved from the satellite images with an average standard deviation of 35% to 54% depending on the model. In term or irradiance value, it rages from 90 to 200 [W/m²] according to the model and the site. The mean bias difference is slightly higher than for the global component, negative for clear conditions and positive for intermediate skies.

As the beam component is derived from the global, the dependances with the different parameters are similar but sharper than for the global irradiance.

9. Conclusions

The first conclusion is that the quality control is a key point in any model validation. Even if the data are highly qualified by the organisation in charge of the acquisition, uncertainties can remain in the data and influence the validation. The best case is when independent data such as aerosol optical depth are available.

The main conclusions of the present study are represented by the first order statistics:

- for latitude from 20° to 60°, altitude from sea level to 1800 m and various climate, the global irradiance is retrieved with a negligible bias and an average standard

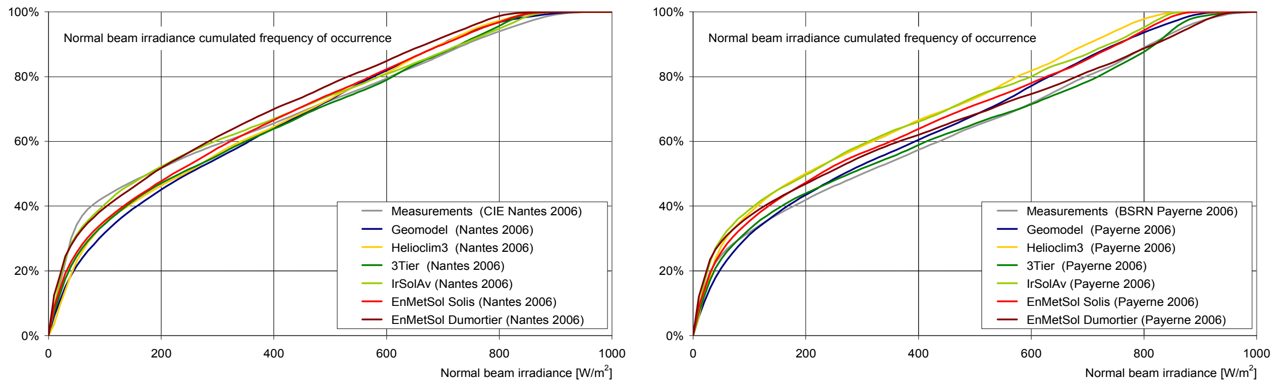

Figure 29 Beam clearness index cumulated frequecy of occurrence for Nantes where the beam is retrieved from the diffuse, and Payerne where the beam componant is acquired.

deviation around 16% for the best algorithm. For the beam irradiance, the bias is around several percents, and the standard deviation around 35%,

- as expected, the main dependance comes from the knowledge of the aerosol optical depth. A lower dependance with the atmospheric water vapor column and the solar elevation angle is pointed out,
- even if the snow cover is taken into account in the algorithm, the sites situated in high altitude such as Junfraujoch and Sonnblick give bad results and are not take into account in the overall statistic.
- the high latitude sites such as Cabauw, Camborne or Toravere give not poorer results than the other sites, only Lerwick, the highest site in latitude (60°N) presents more difficulties. It has also very low levels of irradiance,
- for the majority of the sites, SolarGis and EnMetSol give the best statistics for both of the components.

Neverteless, the interannual variability of the irradiance conditions (it has be shown in a previous study that even for the same site and algorithm, the results can vary from one year to the other, Ineichen 2010a), the lack of independent ground measurements such as aerosol data, the difficulty to assess the exact calibration of the ground data, and the choice of a specific year to carry out the validation, conduct to results that give good indications, but from which it is difficult to draw general conclusions.

10. Acknowledgements

This comparative study could be performed thanks to the data provided by the FluxNet community (http://www.fluxdata.org), the Baseline Surface Radiation Network, the Aeronet network, the CSTB of Nantes and ENTPE in Vaulx-en-Velin, the World Radiation Data Center, and the Swiss Institute of Meteorology.

The derived products where kindly provided by Geomodel in Slovakia, 3Tier in Seattle, the Helioclim data bank in France, University of Oldenburg in Germany, and IrSolAv company in Spain.

11. Nomenclature and abbreviations

I_o	solar constant in W/m^2
B_n	direct normal incidence irradiance in W/m^2
G_h	surface solar global irradiance on a horizontal plane in W/m^2
G_{hc}	clear sky surface solar irradiance in W/m^2
D_h	surface solar diffuse irradiance on a horizontal plane in W/m^2
K_t	global or surface solar irradiance clearness index
K_b	beam clearness index
K_c	clear sky index
K_h	daily global clear sky index
K_{hb}	daily beam clear sky index
n	cloud index
$F_c(G_h)$	cumulated frequecy of occurrence of the global irradiance
h	solar elevation or altitude angle in degrees (°)
AM	optical air mass
RTM	radiative transfer model
T_L	Linke turbidity
aod	aerosol optical depth, or atmospheric aerosol load
T_a	surface (ambient) temperature
HR	relative humidity
w	atmospheric total water vapour column
mbd	mean bias difference
rmsd	root mean square difference
sd	standard deviation
KSI	Kolmogorov-Smirnov index, second order statistic

12. References

Aeronet (AErosol RObotic NETwork) program, http://aeronet.gsfc.nasa.gov/

Atwater M.A., Ball J.T. (1976) Comparison of radiation computations using observed and estimated precipitable water. Appl. Meteorol. 15, 1319-1320

Beyer HG, Costanzo C, Heinemann D (1996): Modications of the Heliosat procedure for irradiance estimates from satellite data. Solar Energy 56, 207–212.

Black J.N., Bonython C.W., Prescott J.A. (1954) *Solar radiation and the duration of sunshine*. Quart. J. Roy. Met. Soc. 80, pp231-235

Dagestad, K. F. and Olseth, J. A., (2007). A modified algorithm for calculating the cloud index. Solar Energy. 81, 280-289.

Derrien M., H. Gleau (2005) MSG/SEVIRI cloud mask and type from SAFNWC, International Journal of Remote Sensing, 26, 4707-4732.

DUMORTIER D (1998): The Satellite model of turbidity variations in Europe. Technical Report

Dürr B., Philipona R, (2004) *Automatic cloud amount detection by surface longwave downward radiation measurements*. J. Geoph. Res., Vol 109

Dürr B. (2006) , personal communication

Espinar B, Ramirez L, Drews D, Beyer H.G, Zarzalejo L.F, Polo J, Martin L. (2009) Analysis of different comparison parameters applied to solar radiation data from satellite and German radiometric stations, *Solar Energy* 83 (2009) 118–125

ESRA (2000) The european solar radiation atlas. Coordinators : K. SCHARMER, J. GREIF, ISBN : 2-911762-21-5

Fontoynont M, Dumortier D et al. (1998) Satellight: A WWW server which provides high quality daylight and solar radiation data for Western and Central Europe. 9th Conference on Satellite Meteorology and Oceanography, 434–437.Frouin R. A., Chertock B., (1992). A technique for global monitoring of net solar irradiance at the ocean surface. Part 1 : Model, *Journal of Applied meteorology,* 31,pp. 1056-1066.

Hammer A, Heinemann D, Hoyer C, Kuhlemann R, Lorenz E, Müller R, Beyer HG (2003): Solar energy assessment using remote sensing technologies. Remote Sensing of Environment, 86, 423–432.

Hammer A, Lorenz E, Kemper A, Heinemann D, Beyer HG, Schumann K, Schwandt M (2009): 'Direct normal irradiance for CSP based on satellite images of Meteosat Second Generation', SolarPACES 2009, Berlin

Helioclim (2009) Sun radiation atlas based on processing of Meteosat data. <http://www.helioclim.net/>

Ineichen P, Perez R. (2002) A new airmass independent formulation for the Linke turbidity coefficient. Solar Energy **73**, No. 3, 151–157

Ineichen P. (2008c). Comparison and validation of three global-to-beam irradiance models against ground measurements. Sol. Energy , doi:10.1016/j.solener.2007.12.006

Ineichen P. (2008a) A broadband simplified version of the Solis clear sky model, Solar Energy 82, pp 758–762

Ineichen P. (2008b) Conversion function between the Linke turbidity and the atmospheric water vapor and aerosol content, Solar Energy 82, pp. 1095–1097

Ineichen P. (2008c). Comparison and validation of three global-to-beam irradiance models against ground measurements. Sol. Energy , doi:10.1016/j.solener.2007.12.006

Ineichen P., Barroso C., Geiger B., Hollmann R., Marsouin A., Mueller R. (2009) Satellite Application Facilities irradiance products: hourly time step comparison and validation over Europe. International Journal of Remote Sensing, Vol. 30, No. 21, pp. 5549–5571

Ineichen P., Perez R. (2010). Aerosol quantification based on global irradiance. Solar paces proceedings, 21-24 sept. Perpignan, France. Available from: http://www.cuepe.ch/html/biblio/pdf/ineichen_2010_aerosol_quantification(SP).pdf

Ineichen P. (2010). Interannual variability and global irradiance evaluation. IEA Task XXXVI report. Available from: http://www.cuepe.ch/html/biblio/pdf/ineichen_2010_05_interannual_variability.pdf

Kalnay E et al. (1996): The NMC/NCAR 40-year reanalysis project. Bull. Am. Meteorol. Soc. 77 (3), 437–472.

Kasten F. (1980) A simple parameterization of two pyrheliometric formulae for determining the Linke turbidity factor. Meteor. Rdsch. **33**, 124–127.

Kinne, S. et al (2005) An AeroCom initial assessment optical properties in aerosol component modules of global models Atmos. Chem. Phys. Discuss., **5**, 1-46.

Linke F. (1922) Transmissions-koeffizient und Trübungsfaktor. Beitr. Phys. Fr. Atmos. 10, pp 91-103.

Liu B.Y.H, Jordan R.C (1960) The interrelationship and characteristic distribution of direct, diffuse and total solar radiation. Volume 4, Issue 3, Pages 1-19

Lorenz E. (2007): Improved diffuse radiation model, MSG. Report for the EC-project PVSAT-2: Intelligent Performance Check of PV System Operation

Louche, A., Notton, G., Poggi, P. and Simonnot, G., (1991). Correlations for direct normal and global horizontal irradiation on a French Mediterranean site. Solar Energy. 46, 261-266.

Mueller R.W. et al, (2004) Rethinking satellite based solar irradiance modelling – The SOLIS clear sky module. Remote Sensing of Environment,**91**, 160-174.

Perez R., R. Seals, P. Ineichen, R. Stewart, D. Menicucci (1987) A New Simplified Version of the Perez Diffuse Irradiance Model for Tilted Surfaces. Description Performance Validation. Solar Energy, 39, 221-232.

Perez R., Ineichen P., Seals R., Zelenka A. (1990) *Making full use of the clearness index for parametrizing hourly insolation conditions*. Solar Energy, Vol. 45, N° 2, pp. 111-114.

Perez R., P. Ineichen, E. Maxwell, R. Seals, A. Zelenka (1992) Dynamic global to direct irradiance conversion models. ASHARE Trans. Res. Series, 1992, 354-369

Perez R., P. Ineichen, K. Moore, M. Kmiecik, C. Chain, R. George, F. Vignola (2002) A New. Operational Satellite-to-Irradiance Model, Solar Energy, 73, 2002, 307-317.

Polo, J., Zarzalejo, L. F., Martin, L., Navarro, A. A. and Marchante, R., (2009a) Estimation of daily Linke turbidity factor by using global irradiance measurements at solar noon. Solar Energy. 83, 1177-1185.

Polo, J., Zarzalejo, L. F., Salvador, P. and Ramírez, L. (2009b) Angstrom turbidity and ozone column estimations from spectral solar irradiance in a semi-desertic environment in Spain. Solar Energy. 83, 257-263.

Randel D., T. H Vonder Haar, M.A. Ringerrud, G. L. Stephens, T.J. Greenwald C.L. Combs (1996) A New Global Water Vapour Dataset. Bulletin of the American Meteorological Society, 77, 1233-1246.

Remund J. (2008), Updated Linke Turbidity and aerosol optical depth climatologies, IEA SHC Task 36 expert meeting, June 2008, Wels, Austria.

Remund J. (2009): Aerosol optical depth and Linke turbidity climatology, Description for final report of IEA SHC Task 36, Meteotest Bern

Rigollier C., Bauer O., Wald L. (2000) On the Clear Sky Model of the ESRA - european Solar Radiation Atlas - with Respect to the Heliosat Method. Solar Energy **68** (1), 33-48.

Rigollier C., Lefèvre M, Wald L. (2004) The method heliosat-2 for deriving shortwave solar irradiance radiation from satellite imagesSolar Energy, 77(2), 159-169

Ruiz-Arias J.A., T. Cebecauer, J. Tovar-Pescador, M. Šúri, (2010). Spatial disaggregation of satellite-derived irradiance using a high resolution digital elevation model, accepted to Solar Energy.

Ruyter de Wildt M., G. Seiz, A. Gruen (2007) Operational snow mapping using multitemporal Meteosat SEVIRI imagery, Remote Sensing of Environment, 109, 29-41.

WMO Publication N° 8 (2008) Guide to Meteorological Instruments and Methods of Observation, ISBN 978-92-63-100085

Zarzalejo, L. F., Polo, J., Martín, L., Ramírez, L. and Espinar, B. (2009). A new statistical approach for deriving global solar radiation from satellite images. Solar Energy. 83, 480-484.

Zelenka A, Perez R, Seals R,Renne D (1999) Effective Accuracy of Satellite-Derived Hourly irradiance. Theor. Appl. Climatol. 62,199-207

Annexe: figures in the following pages:

For the clear, intermediate and overcast sky conditions:

- First and second order statistics in absolute values for the global horizontal irradiance. The sites in grey are not taken into account in the overall statistics.
- First and second order statistics in relative values for the global horizontal irradiance. The sites in grey are not taken into account in the overall statistics.
- First and second order statistics in absolute values for the normal beam irradiance. The sites in grey are not taken into account in the overall statistics.
- First and second order statistics in relative values for the normal beam irradiance. The sites in grey are not taken into account in the overall statistics.

Global irradiance

Clear sky conditions: $0.65 < K'_t \leq 1.00$

	G_h [w/m2]	nb	SolarGis R^2	SolarGis mbd	SolarGis sd	Heliosat 3v3 R^2	Heliosat 3v3 mbd	Heliosat 3v3 sd	3Tier R^2	3Tier mbd	3Tier sd	EnMetSol (Solis) R^2	EnMetSol (Solis) mbd	EnMetSol (Solis) sd	EnMetSol (Dumortier) R^2	EnMetSol (Dumortier) mbd	EnMetSol (Dumortier) sd	IrSolAv R^2	IrSolAv mbd	IrSolAv sd
Cabauw	420	1374	0.980	-17	50	0.983	-33	50	0.976	-24	55	0.986	-23	42	0.985	-25	44			
Camborne	459	1362	0.985	-25	46	0.986	-34	47	0.976	-36	57	0.990	-27	36	0.990	-28	36			
Carpentras	481	2522	0.993	-5	32	0.991	-15	44	0.988	-16	42	0.994	-8	31	0.993	0	34	0.921	-34	107
Davos	517	1775	0.954	-39	76	0.970	-47	64	0.915	-53	109	0.948	-101	81	0.935	-70	92	0.832	-82	148
El Saler	549	2027	0.980	-11	52	0.987	-24	48	0.972	-25	60	0.985	-7	44	0.985	-14	44	0.978	-40	52
Geneva	508	1464	0.983	0	46	0.983	-24	51	0.966	-8	67	0.987	2	40	0.986	12	45	0.957	-25	74
Jungfraujoch	600	1558	0.930	-39	105	0.932	-100	98	0.831	-68	168	0.685	-301	199	0.675	-262	206	0.768	-186	179
Las Majadas	539	2022	0.988	13	42	0.990	-1	43	0.983	12	52	0.991	18	37	0.992	6	35	0.982	-3	51
Lerwick	402	874	0.970	-40	58	0.972	-45	60	0.950	-43	75	0.977	-39	51	0.976	-44	52			
Locarno	512	1813	0.982	-3	44	0.985	-23	52	0.968	-9	63	0.984	-5	42	0.980	-12	47	0.972	-39	55
Nantes	456	1542	0.982	-20	48	0.978	-38	56	0.972	-31	59	0.988	-17	40	0.987	-33	42	0.964	-28	68
Payerne	504	1539	0.977	-13	55	0.972	-46	64	0.964	-22	70	0.980	-14	52	0.979	-4	56	0.958	-36	73
Sede Boqer	662	2285	0.989	-6	38	0.988	-46	41	0.975	-34	59	0.989	-27	41	0.988	-35	43	0.979	-43	55
Sion	535	1851	0.957	-35	71	0.977	-9	58	0.941	-46	83	0.979	-31	50	0.972	-38	57	0.846	-60	133
Sonnblick	481	1837	0.921	-35	99	0.946	-38	83	0.870	-53	134	0.790	-185	150	0.774	-139	162	0.847	-49	140
Tamanrasset	621	3154	0.994	-11	34	0.990	4	51	0.985	-2	55	0.992	-14	39	0.992	-15	37			
Thessaloniki	536	2025	0.989	-7	38	0.988	-34	43	0.971	-30	63	0.978	-28	55	0.977	-30	55	0.973	-29	60
Toravere	400	1545	0.985	-16	41	0.968	-33	68	0.968	-27	58	0.983	-25	43	0.979	-24	48			
Val d'Alinya	578	1532	0.985	-15	48	0.985	-3	57	0.979	-11	60	0.985	-48	49	0.986	-26	47	0.966	11	75
Vaulx-en-Velin	514	1468	0.985	1	43	0.984	-20	47	0.973	-2	59	0.987	3	40	0.987	-4	40	0.973	-16	57
Wien	460	1551	0.981	-12	48	0.983	-33	48	0.972	-22	59	0.986	-22	41	0.986	-12	42	0.956	-29	73
Yatir Forest	626	2523	0.993	-12	33	0.993	-31	40	0.987	-28	45	0.994	-34	29	0.994	-31	31	0.982	-28	51
Zurich	465	1351	0.975	-9	60	0.973	-32	68	0.963	-14	74	0.972	-19	62	0.971	-5	68	0.956	-26	76
All sites	498	35824		-9	43		-23	49		-18	57		-16	41		-16	43		-25	66

Clear sky conditions: first and second order statistics in absolute values for the global horizontal irradiance. The sites in grey are not taken into account in the overall statistics.

	GHI [w/m2]	nb	SolarGis R2	SolarGis mbd%	SolarGis sd%	Heliosat 3v3 R2	Heliosat 3v3 mbd%	Heliosat 3v3 sd%	3Tier R2	3Tier mbd%	3Tier sd%	EnMetSol (Solis) R2	EnMetSol (Solis) mbd%	EnMetSol (Solis) sd%	EnMetSol (Dumortier) R2	EnMetSol (Dumortier) mbd%	EnMetSol (Dumortier) sd%	IrSolAv R2	IrSolAv mbd%	IrSolAv sd%
Cabauw	420	1374	0.980	-4	12	0.983	-8	12	0.976	-6	13	0.986	-5	10	0.985	-6	10			
Camborne	459	1362	0.985	-5	10	0.986	-7	10	0.976	-8	13	0.990	-6	8	0.990	-6	8			
Carpentras	481	2522	0.993	-1	7	0.991	-3	9	0.988	-3	9	0.994	-2	6	0.993	0	7	0.921	-7	22
Davos	517	1775	0.954	-7	15	0.970	-9	12	0.915	-10	21	0.948	-20	16	0.935	-14	18	0.832	-16	29
El Saler	549	2027	0.980	-2	9	0.987	-4	9	0.972	-5	11	0.985	-1	8	0.985	-3	8	0.978	-7	10
Geneva	508	1464	0.983	0	9	0.983	-5	10	0.966	-2	13	0.987	0	8	0.986	2	9	0.957	-5	15
Jungfraujoch	600	1558	0.930	-6	18	0.932	-17	16	0.831	-11	28	0.685	-50	33	0.675	-44	34	0.768	-31	30
Las Majadas	539	2022	0.988	2	8	0.990	0	8	0.983	2	10	0.991	3	7	0.992	1	7	0.982	-1	9
Lerwick	402	874	0.970	-10	14	0.972	-11	15	0.950	-11	19	0.977	-10	13	0.976	-11	13			
Locarno	512	1813	0.982	-1	9	0.985	-5	10	0.968	-2	12	0.984	-1	8	0.980	-2	9	0.972	-8	11
Nantes	456	1542	0.982	-4	11	0.978	-8	12	0.972	-7	13	0.988	-4	9	0.987	-7	9	0.964	-6	15
Payerne	504	1539	0.977	-2	11	0.972	-9	13	0.964	-4	14	0.980	-3	10	0.979	-1	11	0.958	-7	15
Sede Boqer	662	2285	0.989	-1	6	0.988	-7	6	0.975	-5	9	0.989	-4	6	0.988	-5	6	0.979	-7	8
Sion	535	1851	0.957	-7	13	0.977	-2	11	0.941	-9	16	0.979	-6	9	0.972	-7	11	0.846	-11	25
Sonnblick	481	1837	0.921	-7	21	0.946	-8	17	0.870	-11	28	0.790	-38	31	0.774	-29	34	0.847	-10	29
Tamanrasset	621	3154	0.994	-2	6	0.990	1	8	0.985	0	9	0.992	-2	6	0.992	-2	6			
Thessaloniki	536	2025	0.989	-1	7	0.988	-6	8	0.971	-6	12	0.978	-5	10	0.977	-6	10	0.973	-5	11
Toravere	400	1545	0.985	-4	10	0.968	-8	17	0.968	-7	14	0.983	-6	11	0.979	-6	12			
Val d'Alinya	578	1532	0.985	-3	8	0.985	0	10	0.979	-2	10	0.985	-8	9	0.986	-5	8	0.966	2	13
Vaulx-en-Velin	514	1468	0.985	0	8	0.984	-4	9	0.973	0	11	0.987	1	8	0.987	-1	8	0.973	-3	11
Wien	460	1551	0.981	-3	10	0.983	-7	11	0.972	-5	13	0.986	-5	9	0.986	-3	9	0.956	-6	16
Yatir Forest	626	2523	0.993	-2	5	0.993	-5	6	0.987	-4	7	0.994	-6	5	0.994	-5	5	0.982	-4	8
Zurich	465	1351	0.975	-2	13	0.973	-7	15	0.963	-3	16	0.972	-4	13	0.971	-1	15	0.956	-6	16
All sites	498	35824		-2	9		-5	10		-4	11		-3	8		-3	9		-7	17

Clear sky conditions: first and second order statistics in relative values for the global horizontal irradiance. The sites in grey are not taken into account in the overall statistics.

Beam irradiance

Clear sky conditions $0.65 < K'_t \leq 1.00$

	B_n [w/m2]	nb	SolarGis			Heliosat 3v3			3Tier			EnMetSol (Solis)			EnMetSol (Dumortier)			IrSolAv		
			R2	mbd	sd	R2	mbd	sd	R2	mbd	sd	R2	mbd	sd	R2	mbd	sd	R2	mbd	sd
Cabauw	530	1335	0.884	-64	112	0.829	-51	139	0.820	-35	141	0.867	-79	115	0.865	-33	118			
Camborne	556	1195	0.894	-49	109	0.826	-11	141	0.824	-36	144	0.881	-63	114	0.888	-19	109			
Carpentras	652	2522	0.901	-63	100	0.827	-70	141	0.870	-57	119	0.867	-52	115	0.868	-8	116	0.684	-91	202
Davos	676	1775	0.742	-49	202	0.525	-55	263	0.399	-83	328	0.423	-307	288	0.463	-149	306	0.393	-125	348
El Saler																				
Geneva	631	1464	0.805	-51	129	0.775	-83	139	0.750	-20	159	0.815	-43	123	0.834	21	122	0.724	-90	165
Jungfraujoch	381	1558	0.393	363	445	0.325	206	446	0.443	265	440	0.286	-254	444	0.294	-130	460	0.343	46	452
Las Majadas																				
Lerwick	491	790	0.839	-68	138	0.783	-29	170	0.712	-31	190	0.849	-99	134	0.858	-49	130			
Locarno																				
Nantes	595	1542	0.875	-83	107	0.781	-92	147	0.794	-79	144	0.868	-68	108	0.861	-88	107	0.748	-85	168
Payerne	585	1539	0.709	-33	177	0.655	-72	193	0.648	5	210	0.662	-20	189	0.695	42	184	0.629	-60	206
Sede Boqer	757	2247	0.824	-97	101	0.666	-141	153	0.628	-105	148	0.722	-121	126	0.704	-92	134	0.540	-102	171
Sion																				
Sonnblick	518	1837	0.595	150	312	0.405	133	366	0.372	65	402	0.322	-318	364	0.299	-148	418	0.392	82	409
Tamanrasset	706	3154	0.904	-74	112	0.702	24	204	0.733	-41	186	0.756	-33	174	0.790	13	161			
Thessaloniki																				
Toravere	582	1545	0.875	-84	119	0.740	-98	194	0.757	-78	167	0.815	-135	137	0.810	-83	145			
Val d'Alinya																				
Vaulx-en-Velin	643	1468	0.869	-57	99	0.801	-71	120	0.796	-9	134	0.846	-33	105	0.866	-28	101	0.781	-74	136
Wien	541	1551	0.760	-40	159	0.786	-56	151	0.721	-13	176	0.761	-75	154	0.768	6	155	0.707	-65	180
Yatir Forest																				
Zurich																				
All sites	627	20352		-66	121		-61	163		-45	161		-66	138		-24	137		-83	179

Clear sky conditions: first and second order statistics in absolute values for the normal beam irradiance. The sites in grey are not taken into account in the overall statistics.

	B_n [w/m2]	nb	SolarGis			Heliosat 3v3			3Tier			EnMetSol (Solis)			EnMetSol (Dumortier)			IrSolAv		
			R2	mbd%	sd%	R2	mbd%	sd%	R2	mbd%	sd%	R2	mbd%	sd%	R2	mbd%	sd%	R2	mbd%	sd%
Cabauw	530	1335	0.884	-12	21	0.829	-10	26	0.820	-7	27	0.867	-15	22	0.865	-6	22			
Camborne	556	1195	0.894	-9	20	0.826	-2	25	0.824	-6	26	0.881	-11	21	0.888	-3	20			
Carpentras	652	2522	0.901	-10	15	0.827	-11	22	0.870	-9	18	0.867	-8	18	0.868	-1	18	0.684	-14	31
Davos	676	1775	0.742	-7	30	0.525	-8	39	0.399	-12	49	0.423	-45	43	0.463	-22	45	0.393	-18	52
El Saler																				
Geneva	631	1464	0.805	-8	20	0.775	-13	22	0.750	-3	25	0.815	-7	20	0.834	3	19	0.724	-14	26
Jungfraujoch	381	1558	0.393	95	117	0.325	54	117	0.443	70	116	0.286	-67	117	0.294	-34	121	0.343	12	119
Las Majadas																				
Lerwick	491	790	0.839	-14	28	0.783	-6	35	0.712	-6	39	0.849	-20	27	0.858	-10	27			
Locarno																				
Nantes	595	1542	0.875	-14	18	0.781	-15	25	0.794	-13	24	0.868	-11	18	0.861	-15	18	0.748	-14	28
Payerne	585	1539	0.709	-6	30	0.655	-12	33	0.648	1	36	0.662	-3	32	0.695	7	31	0.629	-10	35
Sede Boqer	757	2247	0.824	-13	13	0.666	-19	20	0.628	-14	20	0.722	-16	17	0.704	-12	18	0.540	-14	23
Sion																				
Sonnblick	518	1837	0.595	29	60	0.405	26	71	0.372	12	78	0.322	-61	70	0.299	-29	81	0.392	16	79
Tamanrasset	706	3154	0.904	-10	16	0.702	3	29	0.733	-6	26	0.756	-5	25	0.790	2	23			
Thessaloniki																				
Toravere	582	1545	0.875	-14	21	0.740	-17	33	0.757	-13	29	0.815	-23	23	0.810	-14	25			
Val d'Alinya																				
Vaulx-en-Velin	643	1468	0.869	-9	15	0.801	-11	19	0.796	-1	21	0.846	-5	16	0.866	-4	16	0.781	-11	21
Wien	541	1551	0.760	-7	29	0.786	-10	28	0.721	-2	32	0.761	-14	28	0.768	1	29	0.707	-12	33
Yatir Forest																				
Zurich																				
All sites	627	20352		-10	19		-10	26		-7	26		-10	22		-4	22		-13	29

Clear sky conditions: first and second order statistics in relative values for the normal beam irradiance. The sites in grey are not taken into account in the overall statistics.

Global irradiance

Intermediate sky conditions 0.30 < $K'_t \leq 0.65$

	G_h [W/m^2]	nb	SolarGis			Heliosat 3v3			3Tier			EnMetSol (Solis)			EnMetSol (Dumortier)			IrSolAv		
			R^2	mbd	sd	R^2	mbd	sd	R^2	mbd	sd	R^2	mbd	sd	R^2	mbd	sd	R^2	mbd	sd
Cabauw	252	1578	0.950	-9	54	0.951	-1	60	0.919	0	69	0.970	3	43	0.968	0	44			
Camborne	249	1546	0.941	1	60	0.963	16	58	0.913	2	72	0.962	12	50	0.963	10	49			
Carpentras	267	986	0.937	21	71	0.966	41	68	0.929	12	71	0.964	35	56	0.965	39	59	0.779	27	137
Davos	235	1571	0.851	-5	100	0.948	62	82	0.861	15	101	0.897	-26	81	0.887	-12	87	0.693	-8	141
El Saler	304	1083	0.919	22	82	0.953	37	77	0.908	10	84	0.942	34	70	0.943	29	69	0.898	14	87
Geneva	266	1208	0.935	20	67	0.952	15	67	0.898	10	83	0.958	27	55	0.958	30	58	0.868	19	95
Jungfraujoch	270	1220	0.763	4	146	0.917	123	118	0.773	72	148	0.739	-65	121	0.734	-38	130	0.564	11	189
Las Majadas	292	1036	0.925	34	81	0.957	57	75	0.900	28	90	0.947	56	74	0.949	47	71	0.893	38	93
Lerwick	234	1307	0.933	0	57	0.937	19	74	0.870	13	81	0.938	-7	54	0.938	-10	54			
Locarno	258	1199	0.944	24	64	0.958	50	80	0.928	32	77	0.963	37	56	0.962	33	57	0.901	23	84
Nantes	264	1595	0.958	-1	55	0.938	18	81	0.928	-1	72	0.973	14	46	0.973	4	45	0.896	12	91
Payerne	247	1398	0.942	12	62	0.933	-2	71	0.904	10	79	0.957	21	56	0.957	25	59	0.867	10	92
Sede Boqer	274	522	0.931	30	75	0.946	5	77	0.878	2	89	0.944	28	68	0.944	19	64	0.900	26	86
Sion	224	1437	0.907	-2	75	0.964	62	73	0.905	-1	76	0.953	12	56	0.950	8	58	0.771	3	116
Sonnblick	287	1570	0.765	9	156	0.901	106	125	0.777	54	158	0.767	-51	128	0.761	-15	141	0.661	29	183
Tamanrasset	313	915	0.954	41	80	0.962	95	108	0.921	56	113	0.956	78	98	0.957	76	95			
Thessaloniki	260	1036	0.944	14	69	0.950	8	76	0.921	4	80	0.942	8	69	0.940	8	69	0.900	24	90
Toravere	233	1368	0.941	-7	61	0.945	15	77	0.877	-2	80	0.941	-2	58	0.946	-1	56			
Val d'Alinya	308	637	0.923	42	95	0.940	114	123	0.894	40	110	0.939	38	80	0.940	51	84	0.838	94	143
Vaulx-en-Velin	266	1610	0.955	23	58	0.957	22	64	0.923	22	74	0.968	31	51	0.968	26	52	0.884	22	90
Wien	254	1570	0.931	-2	68	0.937	-6	73	0.920	-2	72	0.958	0	53	0.958	6	55	0.848	3	101
Yatir Forest	325	505	0.899	19	88	0.949	25	72	0.865	6	97	0.943	17	63	0.942	15	64	0.862	11	102
Zurich	259	1560	0.901	16	91	0.910	12	100	0.884	18	97	0.906	16	90	0.908	23	94	0.855	10	108
All sites	249	24096		12	67		22	75		12	80		20	60		19	61		19	95

Intermediate sky conditions: first and second order statistics in absolute values for the global horizontal irradiance. The sites in grey are not taken into account in the overall statistics.

	G_h [W/m^2]	nb	SolarGis			Heliosat 3v3			3Tier			EnMetSol (Solis)			EnMetSol (Dumortier)			IrSolAv		
			R2	mbd%	sd%	R2	mbd%	sd%	R2	mbd%	sd%	R2	mbd%	sd%	R2	mbd%	sd%	R2	mbd%	sd%
Cabauw	252	1578	0.950	-4	22	0.951	0	24	0.919	0	27	0.970	1	17	0.968	0	17			
Camborne	249	1546	0.941	0	24	0.963	6	23	0.913	1	29	0.962	5	20	0.963	4	20			
Carpentras	267	986	0.937	8	26	0.966	15	26	0.929	4	26	0.964	13	21	0.965	15	22	0.779	10	51
Davos	235	1571	0.851	-2	43	0.948	26	35	0.861	7	43	0.897	-11	34	0.887	-5	37	0.693	-4	60
El Saler	304	1083	0.919	7	27	0.953	12	25	0.908	3	28	0.942	11	23	0.943	10	23	0.898	5	29
Geneva	266	1208	0.935	7	25	0.952	6	25	0.898	4	31	0.958	10	21	0.958	11	22	0.868	7	36
Jungfraujoch	270	1220	0.763	1	54	0.917	46	44	0.773	27	55	0.739	-24	45	0.734	-14	48	0.564	4	70
Las Majadas	292	1036	0.925	12	28	0.957	20	26	0.900	10	31	0.947	19	25	0.949	16	24	0.893	13	32
Lerwick	234	1307	0.933	0	24	0.937	8	31	0.870	6	35	0.938	-3	23	0.938	-4	23			
Locarno	258	1199	0.944	9	25	0.958	19	31	0.928	12	30	0.963	14	22	0.962	13	22	0.901	9	33
Nantes	264	1595	0.958	-1	21	0.938	7	31	0.928	0	27	0.973	5	17	0.973	2	17	0.896	5	34
Payerne	247	1398	0.942	5	25	0.933	-1	29	0.904	4	32	0.957	8	23	0.957	10	24	0.867	4	37
Sede Boqer	274	522	0.931	11	27	0.946	2	28	0.878	1	32	0.944	10	25	0.944	7	24	0.900	9	32
Sion	224	1437	0.907	-1	33	0.964	28	33	0.905	0	34	0.953	5	25	0.950	4	26	0.771	1	52
Sonnblick	287	1570	0.765	3	54	0.901	37	44	0.777	19	55	0.767	-18	45	0.761	-5	49	0.661	10	64
Tamanrasset	313	915	0.954	13	25	0.962	30	35	0.921	18	36	0.956	25	31	0.957	24	30			
Thessaloniki	260	1036	0.944	5	26	0.950	3	29	0.921	2	31	0.942	3	26	0.940	3	26	0.900	9	35
Toravere	233	1368	0.941	-3	26	0.945	6	33	0.877	-1	34	0.941	-1	25	0.946	-1	24			
Val d'Alinya	308	637	0.923	14	31	0.940	37	40	0.894	13	36	0.939	12	26	0.940	17	27	0.838	30	46
Vaulx-en-Velin	266	1610	0.955	8	22	0.957	8	24	0.923	8	28	0.968	12	19	0.968	10	19	0.884	8	34
Wien	254	1570	0.931	-1	27	0.937	-2	29	0.920	-1	29	0.958	0	21	0.958	3	22	0.848	1	40
Yatir Forest	325	505	0.899	6	27	0.949	8	22	0.865	2	30	0.943	5	19	0.942	5	20	0.862	3	31
Zurich	259	1560	0.901	6	35	0.910	5	39	0.884	7	37	0.906	6	35	0.908	9	36	0.855	4	42
All sites	249	24096		5	27		9	30		5	32		8	24		8	25		11	53

Intermediate sky conditions: first and second order statistics in relative values for the global horizontal irradiance. The sites in grey are not taken into account in the overall statistics.

Beam irradiance

Intermediate sky conditions $0.30 < K'_t \leq 0.65$

			SolarGis			Heliosat 3v3			3Tier			EnMetSol (Solis)			EnMetSol (Dumortier)			IrSolAv		
	B_n [W/m^2]	nb	R2	mbd	sd	R2	mbd	sd	R2	mbd	sd	R2	mbd	sd	R2	mbd	sd	R2	mbd	sd
Cabauw	122	1568	0.764	14	90	0.680	97	126	0.577	68	148	0.772	38	89	0.754	45	97			
Camborne	104	1293	0.816	54	93	0.759	150	120	0.738	77	130	0.815	66	89	0.810	77	101			
Carpentras	143	986	0.722	74	122	0.729	179	141	0.679	92	152	0.782	109	111	0.779	136	123	0.419	159	240
Davos	76	1571	0.561	111	161	0.566	245	162	0.557	149	191	0.688	24	90	0.675	81	127	0.474	124	197
El Saler																				
Geneva	153	1208	0.725	60	129	0.735	106	128	0.615	88	179	0.791	66	104	0.805	93	115	0.651	85	155
Jungfraujoch	14	1220	0.269	232	243	0.117	461	256	0.203	366	322	0.250	64	110	0.270	138	185	0.160	215	251
Las Majadas																				
Lerwick	82	1230	0.673	52	105	0.570	161	162	0.513	124	175	0.692	40	87	0.662	51	101			
Locarno																				
Nantes	163	1595	0.798	0	91	0.646	88	152	0.684	22	134	0.840	27	83	0.836	14	82	0.646	46	154
Payerne	111	1398	0.675	66	123	0.620	98	138	0.544	108	178	0.711	76	110	0.717	104	124	0.531	89	158
Sede Boqer	272	450	0.659	37	142	0.355	10	200	0.520	40	185	0.541	21	160	0.515	31	170	0.315	78	222
Sion																				
Sonnblick	32	1570	0.401	216	250	0.402	419	242	0.395	308	293	0.451	57	112	0.490	148	189	0.391	262	290
Tamanrasset	124	915	0.721	115	122	0.578	312	212	0.641	184	195	0.606	213	179	0.637	247	173			
Thessaloniki																				
Toravere	131	1368	0.733	3	108	0.726	106	148	0.411	75	193	0.633	21	125	0.694	38	122			
Val d'Alinya																				
Vaulx-en-Velin	206	1592	0.802	27	110	0.704	79	139	0.699	64	159	0.852	45	95	0.860	44	95	0.653	45	154
Wien	152	1570	0.748	24	114	0.748	74	127	0.674	61	149	0.804	26	96	0.792	57	109	0.633	51	155
Yatir Forest																				
Zurich																				
All sites	142	15173		40	110		119	146		81	163		58	108		72	114		73	171

Intermediate sky conditions: first and second order statistics in absolute values for the normal beam irradiance. The sites in grey are not taken into account in the overall statistics.

			SolarGis			Heliosat 3v3			3Tier			EnMetSol (Solis)			EnMetSol (Dumortier)			IrSolAv		
	B_n [W/m^2]	nb	R2	mbd%	sd%	R2	mbd%	sd%	R2	mbd%	sd%	R2	mbd%	sd%	R2	mbd%	sd%	R2	mbd%	sd%
Cabauw	122	1568	0.764	12	74	0.680	80	104	0.577	56	121	0.772	31	73	0.754	37	80			
Camborne	104	1293	0.816	52	90	0.759	144	115	0.738	74	125	0.815	63	86	0.810	74	97			
Carpentras	143	986	0.722	52	85	0.729	125	98	0.679	64	106	0.782	76	78	0.779	94	86	0.419	111	167
Davos	76	1571	0.561	146	211	0.566	322	212	0.557	195	250	0.688	32	118	0.675	106	167	0.474	163	259
El Saler																				
Geneva	153	1208	0.725	39	84	0.735	69	84	0.615	57	117	0.791	43	68	0.805	60	75	0.651	56	101
Jungfraujoch	14	1220	0.269	1660	1743	0.117	3301	1833	0.203	2624	2311	0.250	461	790	0.270	988	1322	0.160	1542	1801
Las Majadas																				
Lerwick	82	1230	0.673	64	129	0.570	197	198	0.513	151	214	0.692	49	107	0.662	62	124			
Locarno																				
Nantes	163	1595	0.798	0	56	0.646	54	93	0.684	13	82	0.840	17	51	0.836	9	50	0.646	28	94
Payerne	111	1398	0.675	60	111	0.620	88	124	0.544	97	160	0.711	68	99	0.717	93	111	0.531	80	142
Sede Boqer	272	450	0.659	14	52	0.355	4	74	0.520	15	68	0.541	8	59	0.515	11	62	0.315	29	82
Sion																				
Sonnblick	32	1570	0.401	680	786	0.402	1317	759	0.395	969	920	0.451	178	352	0.490	466	594	0.391	823	910
Tamanrasset	124	915	0.721	93	99	0.578	252	171	0.641	149	158	0.606	172	145	0.637	200	140			
Thessaloniki																				
Toravere	131	1368	0.733	2	82	0.726	81	113	0.411	57	147	0.633	16	96	0.694	29	93			
Val d'Alinya																				
Vaulx-en-Velin	206	1592	0.802	13	53	0.704	38	67	0.699	31	77	0.852	22	46	0.860	22	46	0.653	22	75
Wien	152	1570	0.748	16	75	0.748	49	84	0.674	40	98	0.804	17	63	0.792	38	72	0.633	34	102
Yatir Forest																				
Zurich																				
All sites	142	15173		28	78		84	103		57	115		41	76		51	81		52	120

Intermediate sky conditions: first and second order statistics in relative values for the normal beam irradiance. The sites in grey are not taken into account in the overall statistics.

Global irradiance

Overcast sky conditions 0.00 < $K'_t \leq 0.30$

	G_h [W/m²]	nb	SolarGis R^2	SolarGis mbd	SolarGis sd	Heliosat 3v3 R^2	Heliosat 3v3 mbd	Heliosat 3v3 sd	3Tier R^2	3Tier mbd	3Tier sd	EnMetSol (Solis) R^2	EnMetSol (Solis) mbd	EnMetSol (Solis) sd	EnMetSol (Dumortier) R^2	EnMetSol (Dumortier) mbd	EnMetSol (Dumortier) sd	IrSolAv R^2	IrSolAv mbd	IrSolAv sd
Cabauw	79	1201	0.879	9	32	0.852	25	48	0.820	38	44	0.907	18	31	0.904	17	31			
Camborne	91	1179	0.866	8	39	0.897	39	59	0.848	31	45	0.898	20	37	0.900	20	37			
Carpentras	77	485	0.803	20	50	0.906	52	52	0.748	32	50	0.879	35	42	0.881	35	42	0.673	71	100
Davos	99	854	0.704	24	72	0.895	128	108	0.775	51	66	0.798	14	53	0.791	25	57	0.485	50	107
El Saler	86	490	0.697	27	68	0.803	41	63	0.627	57	91	0.789	42	61	0.789	40	60	0.594	40	76
Geneva	89	950	0.829	21	46	0.893	23	44	0.803	39	53	0.870	26	40	0.871	27	41	0.653	34	75
Jungfraujoch	105	533	0.632	77	129	0.900	193	155	0.668	148	129	0.611	27	85	0.594	47	98	0.467	102	179
Las Majadas	100	451	0.606	27	77	0.821	89	78	0.561	62	96	0.749	56	72	0.752	52	70	0.647	49	93
Lerwick	85	1125	0.868	27	41	0.873	46	71	0.792	48	55	0.834	17	41	0.839	16	41			
Locarno	64	1172	0.850	35	48	0.848	71	76	0.782	63	69	0.878	36	43	0.877	35	43	0.727	46	73
Nantes	96	1063	0.856	3	37	0.817	45	75	0.837	25	43	0.907	18	32	0.909	14	31	0.650	26	68
Payerne	88	1068	0.813	13	45	0.831	14	51	0.768	37	55	0.881	22	38	0.884	23	38	0.654	34	73
Sede Boqer	118	83	0.579	17	86	0.787	53	89	0.437	89	148	0.697	33	73	0.698	27	71	0.443	24	114
Sion	81	992	0.690	22	67	0.869	114	95	0.800	38	57	0.840	28	49	0.845	26	48	0.555	46	88
Sonnblick	138	526	0.735	71	137	0.747	192	161	0.705	105	148	0.697	32	113	0.686	61	129	0.578	103	178
Tamanrasset	114	224	0.678	33	87	0.865	137	122	0.717	84	112	0.754	90	150	0.754	90	149			
Thessaloniki	91	614	0.751	16	59	0.756	3	61	0.673	42	78	0.774	24	56	0.772	23	56	0.612	39	89
Toravere	79	871	0.830	22	49	0.870	50	75	0.668	47	56	0.818	15	40	0.825	15	39			
Val d'Alinya	97	330	0.762	56	91	0.803	185	143	0.603	101	126	0.791	73	85	0.790	80	90	0.609	111	146
Vaulx-en-Velin	86	1063	0.826	20	45	0.854	35	53	0.789	40	55	0.869	24	40	0.871	20	40	0.627	34	77
Wien	90	1082	0.844	7	40	0.848	6	48	0.811	27	45	0.878	10	36	0.877	12	36	0.637	25	73
Yatir Forest	123	193	0.714	37	93	0.858	81	88	0.624	75	105	0.736	43	77	0.739	40	77	0.574	41	109
Zurich	91	1281	0.760	23	58	0.785	30	74	0.740	50	66	0.769	26	60	0.770	29	63	0.619	39	85
All sites	82	15917		18	49		39	65		42	62		25	48		24	48		36	79

Overcast sky conditions: first and second order statistics in absolute values for the global horizontal irradiance. The sites in grey are not taken into account in the overall statistics.

	G_h [W/m²]	nb	SolarGis R2	SolarGis mbd%	SolarGis sd%	Heliosat 3v3 R2	Heliosat 3v3 mbd%	Heliosat 3v3 sd%	3Tier R2	3Tier mbd%	3Tier sd%	EnMetSol (Solis) R2	EnMetSol (Solis) mbd%	EnMetSol (Solis) sd%	EnMetSol (Dumortier) R2	EnMetSol (Dumortier) mbd%	EnMetSol (Dumortier) sd%	IrSolAv R2	IrSolAv mbd%	IrSolAv sd%
Cabauw	79	1201	0.879	12	41	0.852	31	60	0.820	48	56	0.907	23	39	0.904	21	40			
Camborne	91	1179	0.866	9	43	0.897	43	65	0.848	34	49	0.898	22	41	0.900	22	40			
Carpentras	77	485	0.803	26	65	0.906	67	68	0.748	41	65	0.879	46	54	0.881	45	55	0.673	92	130
Davos	99	854	0.704	24	72	0.895	129	109	0.775	51	67	0.798	14	53	0.791	25	57	0.485	51	107
El Saler	86	490	0.697	31	79	0.803	48	74	0.627	66	106	0.789	49	71	0.789	47	71	0.594	47	89
Geneva	89	950	0.829	24	52	0.893	26	49	0.803	43	59	0.870	29	45	0.871	30	46	0.653	38	84
Jungfraujoch	105	533	0.632	73	123	0.900	184	147	0.668	141	122	0.611	25	81	0.594	44	93	0.467	97	170
Las Majadas	100	451	0.606	27	77	0.821	89	78	0.561	62	96	0.749	56	72	0.752	52	71	0.647	49	93
Lerwick	85	1125	0.868	31	49	0.873	53	83	0.792	56	64	0.834	20	48	0.839	19	48			
Locarno	64	1172	0.850	55	75	0.848	111	119	0.782	99	107	0.878	56	67	0.877	54	66	0.727	72	114
Nantes	96	1063	0.856	3	38	0.817	46	78	0.837	26	45	0.907	19	34	0.909	14	32	0.650	27	71
Payerne	88	1068	0.813	15	51	0.831	16	58	0.768	42	63	0.881	25	43	0.884	26	44	0.654	39	83
Sede Boqer	118	83	0.579	14	73	0.787	45	75	0.437	76	125	0.697	28	62	0.698	23	60	0.443	20	96
Sion	81	992	0.690	28	82	0.869	141	118	0.800	47	71	0.840	35	61	0.845	31	60	0.555	56	109
Sonnblick	138	526	0.735	52	99	0.747	139	117	0.705	77	108	0.697	23	82	0.686	44	94	0.578	75	129
Tamanrasset	114	224	0.678	29	76	0.865	120	107	0.717	73	98	0.754	79	131	0.754	78	131			
Thessaloniki	91	614	0.751	18	65	0.756	3	68	0.673	46	87	0.774	26	62	0.772	25	62	0.612	43	98
Toravere	79	871	0.830	28	62	0.870	63	96	0.668	60	71	0.818	19	50	0.825	19	50			
Val d'Alinya	97	330	0.762	58	94	0.803	192	148	0.603	105	131	0.791	75	88	0.790	83	93	0.609	115	151
Vaulx-en-Velin	86	1063	0.826	24	53	0.854	41	62	0.789	47	64	0.869	28	47	0.871	24	46	0.627	39	89
Wien	90	1082	0.844	8	45	0.848	7	53	0.811	30	50	0.878	12	40	0.877	14	41	0.637	28	82
Yatir Forest	123	193	0.714	30	76	0.858	66	72	0.624	61	85	0.736	35	63	0.739	33	62	0.574	33	88
Zurich	91	1281	0.760	26	63	0.785	33	82	0.740	55	72	0.769	29	66	0.770	31	69	0.619	42	93
All sites	82	15917		22	60		48	80		51	75		30	58		29	59		63	138

Overcast sky conditions: first and second order statistics in relative values for the global horizontal irradiance. The sites in grey are not taken into account in the overall statistics.